Quantum-trajectory Monte Carlo method for internal-state evolution of fast ions traversing amorphous solids

Tatsuya Minami,[1] Carlos O. Reinhold,[1,2] and Joachim Burgdörfer[1,3]
[1]*Department of Physics and Astronomy, University of Tennessee, Knoxville, Tennessee 37996-1200*
[2]*Physics Division, Oak Ridge National Laboratory, Oak Ridge, Tennessee 37831-6372*
[3]*Institute for Theoretical Physics, Vienna University of Technology, A-1040 Vienna, Austria*
(Received 10 October 2002; published 28 February 2003)

We present a theoretical framework for the evolution of the internal state of a fast highly charged one-electron ion traversing an amorphous solid. We employ an open quantum system approach which incorporates the complex array of collisions with electrons and ionic cores in the solid within the framework of system-reservoir interactions. Interactions with the solid environment and the radiation field are treated on the same footing and the quantum master equation for the reduced density matrix of the electronic state of the ion is approximated by a Lindblad equation. The latter allows the solution of this multistate problem in terms of Monte Carlo sampling of quantum trajectories. Similarities and extensions to methods used in quantum optics and previously employed in ion-solid interactions are discussed. Our focus is on the transient buildup and destruction of coherences by stochastic processes. We apply our method to the study of coherence properties of the internal state of a fast Kr^{35+} ion traversing carbon foils. Simulations exhibit clear signatures of partially coherent transitions and are found to be in good agreement with experimental data.

DOI: 10.1103/PhysRevA.67.022902 PACS number(s): 34.50.Fa, 34.10.+x

I. INTRODUCTION

The internal electronic state of a fast atom (or ion) traversing solids is an example of an open quantum system in contact with a ''large reservoir.'' The large number of degrees of freedom of the environment refers here to the electronic and nuclear degrees of freedom of the solid. Moreover, for highly charged ions ($Z_p \gg 1$) the coupling to the vacuum fluctuations of the radiation field become comparable to the coupling to the particles in the solid. Therefore, the reservoir of the open quantum system should include both the radiation field and the degrees of freedom of the solid. We consider in the following a hydrogenic one-electron ion traversing an amorphous carbon foil. For such systems, accurate experimental data [1–4] have recently become available.

Investigations of the electronic excitations in fast ion-solid interactions have remained a theoretical challenge for many decades starting with the early studies by Bohr and Lindhard [5]. The difficulties result not only from the many-body nature of the environment but also from the large number of states of the open system involved that pose a major hurdle for a direct application of a quantum master equation [6–8]. For light ions and weakly bound electrons, a classical transport theory (CTT) [9–11] employing a Monte Carlo sampling of classical trajectories calculated from a microscopic Langevin equation has proven to be quite successful in describing experimental data for electron emission [12,13], charge state fractions and excited state distributions [14,15]. Subsequently, a quantum transport theory (QTT) [4,16,17] was developed in which the reduced density matrix is constructed as a Monte Carlo average of quantum trajectories, each of which is the solution of a Schrödinger equation with a stochastic perturbation. The QTT can be considered as a quantized version of the corresponding CTT. In both the classical as well as the quantum versions of this transport theory, a quasi-free-electron approximation for scattering of electrons at screened ions or conduction electrons was used. For deeply bound electrons in fast highly charged ions, additional quantum effects are expected that originate from the breakdown of the quasi-free-electron approximation [4]. In this regime, also the strong coupling to the radiation field, which scales as ($\propto Z_p^4$), becomes competitive with the collisional coupling, which decreases as $\propto v_p^{-2}$ (v_p being the collision velocity).

Quantum-trajectory Monte Carlo techniques have been independently developed in a different context of quantum optics [18–20] for the description of few-state atomic systems interacting with the radiation field. Quantum trajectories are constructed from a nonlinear stochastic Schrödinger equation (NLSSE) with, in general, non-Hamiltonian interactions. The Monte Carlo solution of the NLSSE is equivalent to a solution of a specific class of quantum master equation for the reduced density operator, the Lindblad equation [21,22], which imposes the condition of complete positivity on the dynamics in the open system. However, the connection between the Lindblad equation and the original master equation it attempts to approximate is far from clear [23–28]. For example, it was shown that the positivity may, in fact, be violated on short time scales [25,27]. The Lindblad equation has been applied mostly to few-state (typically two- or three-state) systems. Generalization of the NLSSE to multistate systems, including unbound states, is not obvious.

In the following, we present a unified description for an open multistate atomic system coupled to both the radiation field and the degrees of freedom of the solid. The starting point of our analysis is the Born-Markov approximation to the quantum master equation, which yields the Redfield equation [29]. Development of a quantum-trajectory Monte Carlo (QTMC) method requires its reduction to a Lindblad form. The standard ''secular approximation'' [30,31] is un-

suitable as it neglects the transient buildup of coherences between nondegenerate states due to stochastic processes, a key feature of high-energy collisions. We therefore develop an alternative approach yielding a Lindblad form that allows the description of coherences on a time scale corresponding to the energy spacing between near-degenerate energy levels. We construct an NLSSE whose quantum Monte Carlo sampling describes the time evolution of the reduced density matrix. This technique allows the treatment of high-dimensional state spaces of the open quantum system. In the limit of weakly bound electrons, our present treatment reduces to the previously developed linear Schrödinger theory with a time-dependent stochastic interaction with the environment. It furthermore possesses a proper classical limit in terms of a classical Langevin equation of motion.

We apply the present theory to the transmission of hydrogenic Krypton ions (Kr^{35+}) through amorphous carbon foils at high velocities ($v_p=47$ a.u.). This system is of particular interest as the time scales for collisional redistribution of states, mixing due to the wake field, spontaneous radiative transitions, level splitting due to the Lamb shift and decoherence are all comparable to each other. We analyze in the following the influence of coherences on the x-ray emission intensities resulting from the transmission and compare our findings with experimental data. A preliminary approach and first results have been presented recently [4]. In that paper the basic ingredients of the QTMC were chosen intuitively rather than determined from first principles, as it is the case in the present formulation. It turns out that our previous implementation can be identified as a limiting case of the present theory when certain additional approximations are invoked.

The structure of the paper is as follows: In Sec. II we briefly review the basic properties of the Lindblad equation and its solution by ensemble averages over trajectories of a nonlinear stochastic Schrödinger equation. The problem of reducing the original master equation in the Born-Markov approximation, usually referred to as Redfield equation, to a Lindblad form will be analyzed in detail in Sec. III. Explicit expressions for the relaxation superoperators for radiative decay, electron-electron scattering, and electron-ionic cores scattering will be given in Sec. IV. The algorithm for the Monte Carlo sampling of the nonlinear stochastic Schrödinger equation will be discussed in Sec. V where we will also analyze its convergence to a Hamiltonian linear Schrödinger equation for high Rydberg states. Numerical results will be given for Kr^{35+} propagating through carbon foils followed by a short summary. Atomic units are used throughout unless otherwise stated.

II. QUANTUM TRAJECTORIES AND THE LINDBLAD EQUATION

In this section we briefly review the basic properties of the Lindblad equation and its solution by a Monte Carlo quantum trajectory technique as they pertain to our description of ion-solid collisions. We consider the interaction of a ''small'' system (S) with a large reservoir (R), also frequently referred to as ''heat bath'' or ''environment.'' The total Hamiltonian is given by

$$\mathbf{H}=H_S+\mathcal{H}_R+\mathbf{V}_{SR}. \tag{2.1}$$

The system in our applications will be the internal state of a fast (velocity $v_p\gg 1$), highly charged (nuclear charge $Z_p\gg 1$) one-electron ion. The system is described by the Hamiltonian H_S, which acts only on the electronic degrees of freedom of the ion. The reservoir will consist of the radiation field as well as charged particles (electrons and ionic cores) of the solid to be taken later as an amorphous carbon foil. In both cases we will consider the reservoir to be in its ground state, (i.e., temperature $T=0$), which is an excellent approximation in view of the energy scales involved. The internal state of the reservoir is described by $\mathcal{H}_R$ (we use calligraphic letters for operators that act only on the reservoir variables). $\mathbf{V}_{SR}$ describes the coupling between the system and respective reservoir (we use bold letters for operators that act on both the system and the reservoir variables).

The time dependence of the density operator $\boldsymbol{\rho}(t)$ is given by the Liouville–von Neumann equation,

$$i\frac{d\boldsymbol{\rho}(t)}{dt}=[\mathbf{H},\boldsymbol{\rho}(t)], \tag{2.2}$$

a solution of which is clearly out of reach for realistic systems. Instead, the focus is on the reduced density operator $\sigma_S(t)$ of the system defined as

$$\sigma(t)=\sigma_S(t)\equiv \mathrm{Tr}_R[\boldsymbol{\rho}(t)]=\sum_i \{i|\boldsymbol{\rho}(t)|i\}, \tag{2.3}$$

where all degrees of freedom of the reservoir have been traced out. We use $|i\},|j\}$, etc. to denote states in the Hilbert space of the reservoir, $\mathbb{H}_R$. Analogously, one can define a reduced density operator of the reservoir, $\sigma_R(t)$,

$$\sigma_R(t)\equiv \mathrm{Tr}_S[\boldsymbol{\rho}(t)]=\sum_\alpha \langle\alpha|\boldsymbol{\rho}|\alpha\rangle, \tag{2.4}$$

where $|\alpha\rangle,|\beta\rangle$, etc. denote states in the Hilbert space of the system, $\mathbb{H}_S$. As the open quantum system approach deals almost exclusively with the density operator σ_S rather than with σ_R, we will drop the subscript S and will use $\sigma(t)=\sigma_S(t)$.

Formulating a master equation of motion for σ is a difficult task. Even in the perturbative limit when the coupling between the system and the reservoir, $\mathbf{V}_{SR}$, is weak, this reduction is nontrivial, as will be analyzed in the following section. The approach proposed by Lindblad [22] starts therefore from a different point of departure. Rather than attempting to construct a reduced equation of motion from Eq. (2.2), it directly postulates an equation based on the principle that the time evolution of σ should be a unitary mapping of the system Hilbert space $\mathbb{H}_S$ onto itself preserving complete positive definiteness (i.e., that $\langle\psi|\sigma|\psi\rangle\geqslant 0$ for any $|\psi\rangle\in\mathbb{H}_S$ and all t),

$$\frac{d\sigma(t)}{dt} = -i[H_S, \sigma(t)] + R^{(L)}\sigma(t), \tag{2.5}$$

where $R^{(L)}$ is the Lindblad relaxation operator describing the interaction of the system with the environment and adopts the form

$$R^{(L)}\sigma(t) = -\frac{1}{2V}\sum_{\vec{k}} [S^\dagger(\vec{k})S(\vec{k})\sigma(t) + \sigma(t)S^\dagger(\vec{k})S(\vec{k}) - 2S(\vec{k})\sigma(t)S^\dagger(\vec{k})]. \tag{2.6}$$

In Eq. (2.6) we have labeled the Lindblad transition operators $S(\vec{k})$ by the index $\vec{k}$ which will later take on the meaning of a wave vector or momentum transfer in collisions (or photon emission). It may also include the summation index over spin or helicity degrees of freedom. The parameter V in Eq. (2.6) denotes the quantization volume for the wave vector. The physical significance of Eq. (2.6) has been extensively debated in the literature (see, e.g., Refs. [23,25,28]). Here we discuss only a few aspects of relevance for the present paper. It is well known that the Lindblad equation cannot be, in general, a faithful representation of the quantum master equation on a time scale comparable to the correlation time τ_c for fluctuations of the reservoir. On the same time scale, the Born-Markov approximation for the weak-coupling limit between system and reservoir underlying most approximate descriptions of the time evolution of $\sigma(t)$ also breaks down. We adopt in this section a pragmatic approach. We take Eq. (2.6) as a useful approximation for the dynamics of the open quantum systems on time scales $t \gg \tau_c$ but comparable to the time scales for the evolution of the atomic degrees of freedom, where expectation values for the atomic observables can meaningfully be extracted.

The importance of the Lindblad equation in the present context is that it can be mapped onto a NLSSE (for details see Ref. [21]), which can be solved by a QTMC technique. Accordingly, the density operator of the system can be constructed from the independent evolution of an ensemble of N_{traj} pure states

$$\sigma(t) = \frac{1}{N_{traj}}\sum_{\eta=1}^{N_{traj}} |\Psi^\eta(t)\rangle\langle\Psi^\eta(t)|, \tag{2.7}$$

where η labels the different stochastic realizations of quantum trajectories $|\Psi^\eta(t)\rangle$. Initially, at $t=0$, each quantum trajectory is placed with probability p_ξ in one of the eigenstates of the initial density matrix, that is, $|\Psi^\eta(0)\rangle = |\xi\rangle$, where $\sigma(0)|\xi\rangle = p_\xi|\xi\rangle$. Expression (2.7) tacitly assumes that an initial ensemble can be uniquely defined irrespective of its coupling to the reservoir. Obviously, preservation of positive definiteness is a condition for the existence of the mapping onto an incoherent superposition of state probabilities.

The equation of motion of $|\Psi^\eta(t)\rangle$ is given by the NLSSE [21],

$$|d\Psi^\eta\rangle = \left\{ -iH_S dt - \frac{dt}{2V}\sum_{\vec{k}} [S^\dagger(\vec{k})S(\vec{k}) - \langle S^\dagger(\vec{k})S(\vec{k})\rangle_\eta] + \frac{1}{V}\sum_{\vec{k}} dN_{\vec{k}}^\eta \left(\frac{S(\vec{k})}{\sqrt{\langle S^\dagger(\vec{k})S(\vec{k})\rangle_\eta}} - 1 \right) \right\} |\Psi^\eta\rangle, \tag{2.8}$$

which is nonlinear in $|\Psi^\eta(t)\rangle$ since the right-hand side explicitly depends on the expectation values $\langle S^\dagger(\vec{k})S(\vec{k})\rangle_\eta = \langle\Psi^\eta(t)|S^\dagger(\vec{k})S(\vec{k})|\Psi^\eta(t)\rangle$. In other words, Eq. (2.8) is not of Hamiltonian form, i.e., $\propto -iH_S dt$. Nonlinearity is also incorporated in the Ito differential $dN_{\vec{k}}^\eta$, a variable that takes the random value 0 or 1 and describes whether or not the system undergoes a stochastic jump during the time interval $(t, t+dt)$. It can be shown that the reduced density-matrix calculated as Monte Carlo average (2.7) yields Lindblad equation (2.5) when the expectation value of the Ito differentials for the system in state $|\Psi^\eta\rangle$ at time t are chosen as

$$\overline{dN_{\vec{k}}^\eta dN_{\vec{k}'}^\eta} = \overline{dN_{\vec{k}}^\eta} V\delta_{\vec{k}\vec{k}'} = dt\langle S^\dagger(\vec{k})S(\vec{k})\rangle_\eta V\delta_{\vec{k}\vec{k}'}. \tag{2.9}$$

The obvious technical advantage of the mapping of the Lindblad master equation onto Eqs. (2.7) and (2.8) is that the computational effort in solving the NLSSE by QTMC methods scales with N_S^2 rather than with N_S^4 for the direct solution of Eq. (2.5), where N_S is the dimension of the state space of the system. As N_S can easily reach $10^2 - 10^3$ for realistic multiple scattering problems, this represents a decisive advantage. Clearly, the price to pay is the additional scaling with N_{traj}, i.e., the number of trajectories required to control the statistical error of the ensemble averaged solution.

The stochastic time evolution of each quantum trajectory is calculated by constructing the corresponding time evolution operator $U^\eta(t,0)$ such that

$$|\Psi^\eta(t)\rangle = U^\eta(t,0)|\Psi^\eta(0)\rangle. \tag{2.10}$$

We decompose the time evolution operator into a sequence of products of two types of evolution operators:

$$U^\eta(t,0) = U_{cont}^\eta(t,t_n)\prod_{j=1}^{n} U_{jump}^\eta(\vec{k}_j,t_j)U_{cont}^\eta(t_j,t_{j-1}), \quad (t_0=0). \tag{2.11}$$

One factor, $U_{jump}^\eta(\vec{k}_j,t_j)$, represents a discontinuous change of the wave function, a stochastic jump, at randomly chosen times $t=t_j$ and index $\vec{k}=\vec{k}_j$. The other factor, $U_{cont}^\eta(t_{j+1},t_j)$, stands for a continuous change of the wave function during the time period $[t_{j+1},t_j]$ between stochastic jumps. The continuous time evolution of the wave function during a time interval between two jumps is given by

$$|\Psi^{\eta}(t_j)\rangle = U^{\eta}_{cont}(t_j,t_{j-1})|\Psi^{\eta}(t_{j-1})\rangle = \frac{\exp[-iH_{eff}(t_j-t_{j-1})]|\Psi^{\eta}(t_{j-1})\rangle}{||\exp[-iH_{eff}(t_j-t_{j-1})]|\Psi^{\eta}(t_{j-1})\rangle||} \tag{2.12}$$

with

$$H_{eff} = H_S - i\frac{\Gamma}{2}, \tag{2.13}$$

where the decay operator Γ is given by

$$\Gamma = \frac{1}{V}\sum_{\vec{k}} S^{\dagger}(\vec{k})S(\vec{k}). \tag{2.14}$$

The effective, non-Hermitian Hamiltonian of the system, H_{eff}, includes the effect of decay due to the coupling to the reservoir [21] through the decay operator Γ. Since H_{eff} is non-Hermitian, Eq. (2.12) is often referred to as nonunitary evolution. In fact, due to the renormalization of the state vector $|\Psi^{\eta}(t_j)\rangle$ by means of the denominator, U^{η}_{cont} corresponds to a unitary ''rotation'' of the state vector in the Hilbert space $\mathbb{H}_S$. The underlying physical picture is that due to differences in coupling strength of the different eigenstates of H_S to the environment, the net effect of the continuous evolution is the change in phase and relative weight of the expansion coefficients of $|\Psi^{\eta}\rangle$ in terms of the eigenstates of H_S. Continuous evolution operator (2.12) accounts for the first term of Lindblad equation (2.5) and the first two terms of Lindblad relaxation superoperator (2.6).

Stochastic jumps at the time t_j for a given value of $\vec{k} = \vec{k}_j$ are described by the operators $U^{\eta}_{jump}(\vec{k}_j,t_j)$ defined by

$$|\Psi^{\eta}(t_j+\delta t)\rangle = U^{\eta}_{jump}(\vec{k}_j,t_j)|\Psi^{\eta}(t_j)\rangle = \frac{S(\vec{k}_j)|\Psi^{\eta}(t_j)\rangle}{||S(\vec{k}_j)|\Psi^{\eta}(t_j)\rangle||}, \tag{2.15}$$

where $\delta t \to 0$ is an infinitesimal time step. The jump operator simulates the effect of the last term of Lindblad relaxation operator (2.6), often referred to as the gain or source term. Since U^{η}_{jump} is proportional to S, we refer to the latter for simplicity also as ''jump'' operator.

The basic ingredients of the Monte Carlo algorithm that determine the operators U^{η}_{cont} and U^{η}_{jump} are the random jump times t_j and the random value of $\vec{k}_j$ in Eq. (2.15). In order for the Monte Carlo algorithm to yield the correct NLSSE, these random variables must be chosen such that the average number of jumps per infinitesimal time steps δt yields Eq. (2.9). As is usual in sampling random numbers from multidimensional distributions, one first samples the value of t_j and, subsequently, one samples the value of $\vec{k}_j$ from the conditional probability density

$$P^{\eta}(\vec{k}_j)|_{t=t_j} = \frac{||S(\vec{k}_j)|\Psi^{\eta}(t_j)\rangle||^2}{V^{-1}\sum_{\vec{k}} ||S(\vec{k})|\Psi^{\eta}(t_j)\rangle||^2}. \tag{2.16}$$

From Eq. (2.9), the probability density of jump times $\varrho^{\eta}(t_j)$ must obey

$$\int_{t_{j-1}}^{t_{j-1}+\delta t} \varrho^{\eta}(t_j)dt_j = \delta t\langle\Gamma\rangle_{\eta} = \delta t\langle\Psi^{\eta}(t_{j-1})|\Gamma|\Psi^{\eta}(t_{j-1})\rangle. \tag{2.17}$$

The most natural choice obeying Eq. (2.17) consists of

$$\varrho^{\eta}(t_j) = \frac{d}{dt}||\exp[-iH_{eff}(t_j-t_{j-1})]|\Psi^{\eta}(t_{j-1})\rangle||^2. \tag{2.18}$$

Since the integral of any probability density has a uniform distribution in the interval (0,1), the random jump time t_j can be obtained from the implicit equation

$$u = 1 - ||e^{-iH_{eff}(t_j-t_{j-1})}|\Psi^{\eta}(t_{j-1})\rangle||^2, \tag{2.19}$$

where u is a uniformly distributed random number, $u \in [0,1]$.

III. LINDBLAD APPROXIMATION OF THE REDFIELD EQUATION

In this section we analyze the approximate reduction of the quantum master equation in Born-Markov approximation to a Lindblad form. We emphasize that such a reduction is not unique and requires additional approximations. The figure of merit for our proposed approximation is the degree to which the resulting Lindblad form is capable of reproducing the time evolution of atomic coherences on time scales long compared to the reservoir correlation time τ_c but short compared to the time scale of the secular motion of the atomic population. Such an analysis appears to be missing for true multistate problems such as excitation by multiple scattering.

The starting point of our analysis is Liouville–von Neumann equation (2.2) for the total density operator which can be rewritten in the interaction (I) representation as an integrodifferential equation

$$i\frac{d}{dt}\boldsymbol{\rho}^I(t) = [\mathbf{V}^I_{SR}(t),\boldsymbol{\rho}^I(0)] - i\int_0^t dt'[\mathbf{V}^I_{SR}(t),[\mathbf{V}^I_{SR}(t'),\boldsymbol{\rho}^I(t')]]. \tag{3.1}$$

The transformation to the interaction representation of any Schrödinger operator $\mathbf{O}$ is given by the total evolution operator of the unperturbed system plus reservoir

$$\mathbf{O}^I = e^{i(H_S+\mathcal{H}_R)t}\mathbf{O}e^{-i(H_S+\mathcal{H}_R)t}. \tag{3.2}$$

The Born-Markov approximation to Eq. (3.1) involves the following assumptions (see, e.g., Ref. [23]).

(i) The initial density operator at time $t=0$ is given by a tensor product of σ and σ_R,

$$\boldsymbol{\rho}^I(0)=\sigma^I(0)\otimes\sigma_R^I(0). \tag{3.3}$$

This assumption can be justified when the interaction $\mathbf{V}_{SR}$ is switched off for $t<0$. Otherwise, the system-reservoir coupling will lead to an entanglement between the system and the reservoir degrees of freedom and a break down of the factorization Eq. (3.3). In our present study, the interaction between the atomic system and the solid is switched on only as the fast projectile penetrates the entrance surface of the solid, taken to be $t=0$. By the same token, the initial state of the system will be assumed to be the ground-state and the initial-state decay due to the coupling to the radiation field can be neglected for $t<0$. Therefore, Eq. (3.3) appears to be a good approximation.

(ii) The coupling $\mathbf{V}_{SR}$ is assumed to be sufficiently ''weak'' as to allow the evolution of the reservoir to be unaffected by the interaction with the system. This implies that

$$\sigma_R^I(t)=\sigma_R^I(0)=\sigma_R(0) \tag{3.4}$$

and, furthermore, that

$$\boldsymbol{\rho}^I(t)=\sigma^I(t)\otimes\sigma_R^I(0), \tag{3.5}$$

i.e., the factorization Eq. (3.3) remains valid for all future times. The latter can only be correct to order $O(\mathbf{V}_{SR})$ since the perturbation will generate transient entanglement between the system and the reservoir variables. This is the origin of the failure of the Born-Markov approximation on short time scales of the order of τ_c before rapid fluctuations in the reservoir destroy the entanglement in the ''coarse-grained'' evolution [23,25]. In the present case, the order parameter of the strength of the interaction is given for the collisional interaction by the inverse transmission speed, $v_p^{-1}\ll 1$, and by $Z_p\alpha\ll 1$ for the radiative interaction, where α is the fine structure constant. Assumption (ii) corresponds to assuming the linear response of reservoir variables. It should be noted, however, that no such assumption is implied for the degrees of freedom of the system. Under these assumptions and tracing out the reservoir degrees of freedom in Eq. (3.1) the equation of motion for the reduced density matrix $\sigma(t)$ becomes

$$i\frac{d}{dt}\sigma^I(t)=-i\int_0^t d\tau \times \mathrm{Tr}_R\{\mathbf{V}_{SR}^I(t),[\mathbf{V}_{SR}^I(t-\tau),\sigma^I(t-\tau)\otimes\sigma_R^I]\}, \tag{3.6}$$

where $\tau=t-t'$ and we have assumed that the commutators linear in $\mathbf{V}_{SR}^I$ vanish

$$\mathrm{Tr}_R[\mathbf{V}_{SR}^I(t),\sigma^I(0)\otimes\sigma_R^I]=0. \tag{3.7}$$

Equation (3.7) does not pose serious restrictions on the validity of the approach. If Eq. (3.7) does not hold, the corresponding contributions can be included in the unperturbed Hamiltonian H_S.

We choose now a class of system-reservoir interactions which can be written as a bilinear form with factors acting on either the reservoir or the system degrees of freedom,

$$\mathbf{V}_{SR}(t)=\frac{1}{2V}\sum_{\vec{k}}\,[e^{i\vec{k}\vec{v}_p t}f(\vec{k})W(\vec{k})\mathcal{B}^\dagger(\vec{k})+\mathrm{H.c.}] =\frac{1}{V}\sum_{\vec{k}}\,e^{i\vec{k}\vec{v}_p t}f(\vec{k})W(\vec{k})\mathcal{B}^\dagger(\vec{k}), \tag{3.8}$$

where the W operators act on the system Hilbert space $\mathbb{H}_S$, the $\mathcal{B}$ operators act on the reservoir Hilbert space $\mathbb{H}_R$, $f(\vec{k})$ is a scalar function, and the abbreviation H.c. means Hermitian conjugate. In order for the last identity in Eq. (3.8) to hold, we have assumed that $f(-\vec{k})=f^*(\vec{k})$, $W(-\vec{k})=W^\dagger(\vec{k})$, and $\mathcal{B}(-\vec{k})=\mathcal{B}^\dagger(\vec{k})$ so that the inverse Fourier transform of $f(\vec{k})$ is a real function and that of $W(\vec{k})$ and $\mathcal{B}(\vec{k})$ are Hermitian operators. The boost operator $\exp(i\vec{k}\cdot\vec{v}_p t)$ in Eq. (3.8) accounts for the Galilei shift between the rest frame of the reservoir (the solid) and the system (the moving ion). Clearly, for the interaction with the vacuum fluctuations of the radiation field $v_p=0$. Both charged-particle interactions and the interaction with the radiation field are of the form Eq. (3.8). Explicit expressions for $W(\vec{k})$ and $\mathcal{B}(\vec{k})$ will be given below.

Inserting Eq. (3.8) into Eq. (3.6) leads to

$$\begin{aligned} i\frac{d}{dt}\sigma^I(t)=\frac{1}{V}\sum_{\vec{k}}\,\int_0^t d\tau|f(\vec{k})|^2 &\times\{e^{-i\vec{k}\vec{v}_p\tau}W^{I\dagger}(\vec{k},t)W^I(\vec{k},t-\tau)\sigma^I(t-\tau)G(\vec{k},\tau) \\ &-e^{i\vec{k}\vec{v}_p\tau}\sigma^I(t-\tau)W^{I\dagger}(\vec{k},t-\tau)W^I(\vec{k},t)G^*(\vec{k},\tau) \\ &+e^{i\vec{k}\vec{v}_p\tau}W^I(\vec{k},t)\sigma^I(t-\tau)W^{I\dagger}(\vec{k},t-\tau)G^*(\vec{k},\tau) \\ &-e^{-i\vec{k}\vec{v}_p\tau}W^I(\vec{k},t-\tau)\sigma^I(t-\tau)W^{I\dagger}(\vec{k},t)G(\vec{k},\tau)\}. \end{aligned} \tag{3.9}$$

In Eq. (3.9), $G(\vec{k},\tau)$ denotes the retarded Green's function for the reservoir variable $\mathcal{B}(\vec{k})$

$$\begin{aligned} V\delta_{\vec{k},\vec{k}'}G(\vec{k},\tau)&=-i\,\theta(\tau)\mathrm{Tr}_R[\sigma_R^I\mathcal{B}^I(\vec{k},t)\mathcal{B}^{I\dagger}(\vec{k}',t-\tau)] \\ &=-i\,\theta(\tau)\mathrm{Tr}_R[\sigma_R^I\mathcal{B}(\vec{k})e^{-i\mathcal{H}_R\tau}\mathcal{B}^\dagger(\vec{k}')e^{i\mathcal{H}_R\tau}], \end{aligned} \tag{3.10}$$

where $\theta(\tau)$ is the Heaviside step function. The Kronecker δ in Eq. (3.10) expresses the translational invariance assumed for the reservoir. The advanced Green's function is correspondingly given by $G^A(\vec{k},\tau)=G^*(\vec{k},-\tau)$.

An explicit form of the Green's function can be obtained using an expansion over the eigenstates $|n\}$ of the reservoir defined by $H_R|n\}=E_n|n\}$. Specializing in the following to the case where the reservoir is in the ground state $|0\}$ (or, equivalently, in the zero temperature limit), i.e., $\{n|\sigma_R^I|m\}=\delta_{0,n}\delta_{0,m}$ we have

$$G(\vec{k},\tau) = -i\,\theta(\tau)\sum_n |\{0|\mathcal{B}(\vec{k})|n\}|^2 e^{-i\Omega_{n0}\tau}, \quad (3.11)$$

with all $\Omega_{n0}=E_n-E_0$ positive, signifying the fact that the reservoir can only be a sink rather than a source of excitation energy. Equation (3.11) applies to both the radiation field and the solid considered as environment.

We now turn to the Markov approximation of Eq. (3.9). The excitation spectrum $\{\Omega_{n0}\}$ of the reservoir system is considered to be sufficiently broad as to render $G(\vec{k},\tau)$ as a function of τ to be rapidly decaying over a characteristic relaxation time τ_c, which is usually called the correlation time [note that retarded Green's function (3.10) for $\mathcal{B}(k)$ is closely related to its autocorrelation function]. The ''rapid'' decay of Green's function is to be measured on the time scale of typical changes of the reduced density matrix of the system such that

$$\sigma(t-\tau_c)\simeq\sigma(t). \quad (3.12)$$

Approximation (3.12) is usually referred to as loss of memory since the evolution of $\sigma(t)$ is assumed to depend only on the instantaneous values of $\sigma(t)$ rather than its past. If such an approximation applies, the time integral over τ in Eq. (3.9) can be extended to infinity. Estimates for the rate of change of $\sigma(t)$ can be taken from Fermi's golden rule (setting $\tau\simeq 0$ in Eq. (3.9) in the arguments of W^I, G, and σ^I). Provided that the system is initially in a pure state $|\alpha\rangle$, the validity of Eq. (3.12) requires that the relative change of $\sigma_{\alpha\alpha}=\langle\alpha|\sigma|\alpha\rangle$ is small compared to the inverse correlation time of the reservoir, i.e.,

$$\left|\frac{\frac{d}{dt}\sigma_{\alpha\alpha}(t)}{\sigma_{\alpha\alpha}(t)}\right| = \left|\frac{\frac{d}{dt}\sigma^I_{\alpha\alpha}(t)}{\sigma^I_{\alpha\alpha}(t)}\right| \ll \frac{1}{\tau_c}. \quad (3.13)$$

The relative change of $\sigma^I_{\alpha\alpha}$ due to, e.g., the first term in Eq. (3.9) can be estimated to be of the order of

$$\left|\frac{\frac{d}{dt}\sigma^I_{\alpha\alpha}(t)}{\sigma^I_{\alpha\alpha}(t)}\right| \simeq \frac{2}{V}\sum_{\beta,\vec{k}} |f(\vec{k})|^2 |W^I_{\beta\alpha}(\vec{k})|^2 |G(\vec{k},0)| \times \frac{|\sin(\vec{v}_p\vec{k}\tau_c/2)|}{|\vec{v}_p\vec{k}|}, \quad (3.14)$$

where the sum over β runs over a complete set of states in the Hilbert space of the system [other terms in Eq. (3.9) can be treated analogously]. Consider first the case $v_p=0$, i.e., the absence of the Galilei shift of the reservoir which applies to the interaction with the radiation field. Eq. (3.13) reduces to

$$\left(\frac{1}{V}\sum_{\beta,\vec{k}} |f(\vec{k})|^2 |W^I_{\beta\alpha}(\vec{k})|^2 |G(\vec{k},0)|\right)\tau_c^2 \ll 1. \quad (3.15)$$

The prefactor to τ_c^2 in Eq. (3.15) is of the order of the transition rate in the Born approximation (i.e., Fermi's golden rule), which, from the outset, was assumed to be small. Therefore, Eq. (3.15) poses only a fairly mild constrain on τ_c. Consider now the case of fast collisions $v_p \gg 1$. Using the upper bound $|\sin(\vec{v}_p\vec{k}\tau_c/2)|\leqslant 1$, Eq. (3.13) becomes

$$\left(\frac{2}{V}\sum_{\beta,\vec{k}} \frac{|f(\vec{k})|^2 |W^I_{\beta\alpha}(\vec{k})|^2 |G(\vec{k},0)|}{|\vec{v}_p\vec{k}|}\right)\tau_c \ll 1. \quad (3.16)$$

For $v_p\to\infty$ the prefactor to τ_c becomes small irrespective of the size of W or G. This is directly related to the fact that the Born approximation is valid for collisions at high speeds due to the short interaction time even if the (static) perturbation is not weak. The point to be noted is that neither Eq. (3.15) nor Eq. (3.16) require τ_c to be short on the fast internal time scale of the system. The latter is of crucial importance for highly charged ions, where classical orbital periods (or inverse transition frequencies) are short and scale as $\propto Z_p^{-2} \ll 1$. Since for environments of charged particles, for example an electron gas at metallic densities, typical correlation times τ_c are of the order of one a.u., it is the high speed that renders the Markov approximation to be valid.

Using Eq. (3.12) in Eq. (3.9) and projecting onto eigenstates $|\alpha\rangle$ of the unperturbed system (i.e., $H_S|\alpha\rangle=\varepsilon_\alpha|\alpha\rangle$) leads to

$$\begin{aligned} i\frac{d}{dt}\sigma^I_{\alpha\beta}(t) = \frac{1}{V}\sum_{\vec{k}} |f(\vec{k})|^2 \sum_{\nu,\mu} \{ & e^{i\omega_{\alpha\mu}t} W^\dagger_{\alpha\nu}(\vec{k}) W_{\nu\mu}(\vec{k}) \sigma^I_{\mu\beta}(t) \\ & \times \tilde{G}(\vec{k},\omega_{\mu\nu}-\vec{v}_p\vec{k}) - e^{i\omega_{\nu\beta}t}\sigma^I_{\alpha\nu}(t) W^\dagger_{\nu\mu}(\vec{k}) \\ & \times W_{\mu\beta}(\vec{k}) \tilde{G}^*(\vec{k},-(\omega_{\mu\nu}+\vec{v}_p\vec{k})) \\ & + e^{i(\omega_{\alpha\nu}-\omega_{\beta\mu})t} W_{\alpha\nu}(\vec{k}) \sigma^I_{\nu\mu}(t) W^\dagger_{\mu\beta}(\vec{k}) \\ & \times [\tilde{G}^*(\vec{k},-(\omega_{\beta\mu}+\vec{v}_p\vec{k})) - \tilde{G}(\vec{k},\omega_{\nu\alpha}-\vec{v}_p\vec{k})]\}, \end{aligned} \quad (3.17)$$

where $\omega_{\alpha\beta}=\varepsilon_\alpha-\varepsilon_\beta$. The function $\tilde{G}(\vec{k},\omega)$ results from the time integral over τ and corresponds to the Fourier transform of Green's function $G(\vec{k},\tau)$,

$$\tilde{G}(\vec{k},\omega) = \int_{-\infty}^{\infty} d\tau e^{i\omega\tau} G(\vec{k},\tau) = \lim_{\delta\to 0}\sum_n \frac{|\{0|\mathcal{B}(\vec{k})|n\}|^2}{\omega-\Omega_{n0}+i\delta}, \quad (3.18)$$

whose real and imaginary parts adopt the forms

$$\mathrm{Re}(\tilde{G}(\vec{k},\omega)) = \sum_n |\{0|\mathcal{B}(\vec{k})|n\}|^2 \,\mathrm{P}\left(\frac{1}{\omega-\Omega_{n0}}\right), \quad (3.19)$$

$$\mathrm{Im}(\tilde{G}(\vec{k},\omega)) = -\pi\sum_n |\{0|\mathcal{B}(\vec{k})|n\}|^2 \delta(\omega-\Omega_{n0}) \quad (3.20)$$

and P denotes the principal part.

The real part of $\tilde{G}$ describes the energy shift due to the virtual transitions in the reservoir. That is, the first two terms of Eq. (3.17) involving $\mathrm{Re}(\tilde{G})$ yield a contribution to the master equation of σ that has the form of a commutator $[\Delta H,\sigma]$, where

$$\Delta H_{\alpha\mu}=\frac{1}{V}\sum_{\vec{k}}|f(\vec{k})|^2\sum_{\nu}W^{\dagger}_{\alpha\nu}(\vec{k}) \times W_{\nu\mu}(\vec{k})\mathrm{Re}(\tilde{G}(\vec{k},\omega_{\mu\nu}-\vec{v}_p\vec{k})) \tag{3.21}$$

represents a Hermitian shift of the original Hamiltonian H_S. Physical realizations of this shift are the Lamb shift for the radiation field or the charge-density fluctuation induced energy shift of the projectile electron. Rather than dealing explicitly with contributions associated with $\mathrm{Re}(\tilde{G})$, we will assume in the following that ΔH is already taken into account from the onset in the Hamiltonian of the system H_S in Eq. (2.1). This allows us to include the shift more accurately than Eq. (3.21) (either via an independent higher-order calculation or experimental data) and, moreover, it allows to incorporate the energy shifts to all orders in the time evolution through the phases $\exp[-i(\varepsilon_\alpha^{(0)}+\Delta\varepsilon_\alpha)t]$. For consistency reasons, we will remove all terms involving $\mathrm{Re}(\tilde{G})$ and assume from now on that only terms containing $\mathrm{Im}(\tilde{G})$ contribute to the right-hand side of Eq. (3.17).

The imaginary part of $\tilde{G}$ is directly related to the dynamic susceptibility χ of the environment. According to linear response theory, the relation between these two quantities is [31]

$$\chi(\omega)=\frac{1}{V}\sum_{\vec{k}}\chi(\vec{k},\omega)=\frac{1}{V}\sum_{\vec{k}}[\tilde{G}(\vec{k},\omega)-\tilde{G}^*(\vec{k},-\omega)]. \tag{3.22}$$

Using Eq. (3.20) and separating χ into its real and imaginary parts as $\chi=\chi'-i\chi''$,

$$\chi''(\vec{k},\omega)=\pi\sum_n|\{0|\mathcal{B}(\vec{k})|n\}|^2[\delta(\omega-\Omega_{n0})+\delta(\omega+\Omega_{n0})]. \tag{3.23}$$

Consequently, we obtain

$$-\mathrm{Im}[\tilde{G}(\vec{k},\omega)]=\chi''_+(\vec{k},\omega)=\theta(\omega)\chi''(\vec{k},\omega). \tag{3.24}$$

The step function $\theta(\omega)$ (and the subindex $+$) signifies the exothermicity condition of the allowed transitions of the environment, which is initially in its ground state (i.e., $\Omega_{n0}>0$).

Transforming σ^I in Eq. (3.17) from the interaction representation back to the Schrödinger representation and using Eq. (3.24) results in the Redfield equation [29,31]

$$\begin{aligned}\frac{d}{dt}\sigma_{\alpha\beta}(t)=&-i\omega_{\alpha\beta}\sigma_{\alpha\beta}(t)-\frac{1}{V}\sum_{\vec{k}}|f(\vec{k})|^2\\ &\times\sum_{\nu,\mu}\{W^{\dagger}_{\alpha\nu}(\vec{k})W_{\nu\mu}(\vec{k})\sigma_{\mu\beta}(t)\chi''_+(\vec{k},\omega_{\mu\nu}-\vec{v}_p\vec{k})\\ &+\sigma_{\alpha\nu}(t)W^{\dagger}_{\nu\mu}(\vec{k})W_{\mu\beta}(\vec{k})\chi''_+(\vec{k},\omega_{\nu\mu}-\vec{v}_p\vec{k})\\ &-W_{\alpha\nu}(\vec{k})\sigma_{\nu\mu}(t)W^{\dagger}_{\mu\beta}(\vec{k})[\chi''_+(\vec{k},\omega_{\nu\alpha}-\vec{v}_p\vec{k})\\ &+\chi''_+(\vec{k},\omega_{\mu\beta}-\vec{v}_p\vec{k})]\}.\end{aligned} \tag{3.25}$$

This equation can be formally written in matrix form as Lindblad equation (2.5). The crucial point is now that the resulting Redfield relaxation operator $R^{(R)}$ does not possess the same structure as Lindblad relaxation operator (2.6). The Lindblad equation, in turn, corresponds to a system of coupled equations

$$\frac{d\sigma_{\alpha\beta}}{dt}=-i\omega_{\alpha\beta}\sigma_{\alpha\beta}+\sum_{\mu,\nu=1}^{N_s}R^{(L)}_{\alpha\beta\mu\nu}\sigma_{\mu\nu}, \tag{3.26}$$

where the "couplings" $R^{(L)}_{\alpha\beta\mu\nu}$ have the form

$$R^{(L)}_{\alpha\beta\mu\nu}=-\frac{1}{2}(\delta_{\nu\beta}\Gamma_{\alpha\mu}+\delta_{\alpha\mu}\Gamma_{\nu\beta})+\frac{1}{V}\sum_{\vec{k}}S_{\alpha\mu}(\vec{k})S^{\dagger}_{\nu\beta}(\vec{k}), \tag{3.27}$$

Mapping Eq. (3.25) onto Eqs. (3.26)–(3.27) involves additional approximations which have profound consequences as to the regime within which the Lindblad equations can be applied. The standard approximation utilized in the literature to reach a Lindblad form is the so-called "secular approximation" [2,30,31] (in the quantum optics context sometimes also referred to as the rotating wave approximation [28]). It assumes that all terms on the right-hand side of Eq. (3.17) which carry an oscillatory phase factor average out and hence only diagonal terms survive. The secular approximation follows from Eq. (3.17) by replacing all complex exponentials by Kronecker δ functions, e.g.,

$$e^{i\omega_{\nu\beta}t}=\delta_{\epsilon_\nu,\epsilon_\beta}=\delta_{\nu,\beta}, \tag{3.28}$$

$$e^{i(\omega_{\alpha\nu}-\omega_{\beta\mu})t}=\delta_{\omega_{\alpha\nu},\omega_{\beta\mu}}=\delta_{\alpha,\beta}\delta_{\nu\mu}, \tag{3.29}$$

where the last equalities hold when the spectrum is nondegenerate. As the interaction with the environment induces small energy splittings in the frequency spectrum of the system through $\mathrm{Re}(\tilde{G})$ to be included in H_S [see below Eq. (3.21)], many degeneracies are removed. In the nondegenerate case, the secular approximation leads to a total decoupling between the diagonal and off-diagonal matrix elements of the density matrix. While the populations obey a system of coupled rate equations

$$\frac{d}{dt}\sigma_{\alpha\alpha}(t)=\sum_{\nu}R^{secular}_{\alpha\alpha\nu\nu}\sigma_{\nu\nu}(t), \tag{3.30}$$

the time evolution of coherences is governed by a set of independent decay equations

$$\frac{d}{dt}\sigma_{\alpha\beta}(t)=(-i\omega_{\alpha\beta}+R^{secular}_{\alpha\beta\alpha\beta})\sigma_{\alpha\beta}(t), \tag{3.31}$$

where $\alpha\neq\beta$ and $R^{secular}_{\alpha\beta\sigma\beta}$ is negative definite. The secular approximation does not allow for the production of coherences between different unperturbed energy eigenstates due to the interaction with the environment but allows only for its decay. This result is, however, only valid for the long time scale $t\gg t_I=2\pi/|\omega_{\alpha\beta}|$ for decoherence due to dephasing. In turn, on an intermediate time scale

$$\tau_c\ll t\leqslant t_I \tag{3.32}$$

transient coherences caused by interactions with the environment can play an important role, an example of which is the internal state evolution in transport through solids. Another example is spontaneous radiative decay, where the buildup of transient coherences can occur [30] but has been mostly ignored in the context of Lindblad equations.

Our reduction of the Redfield equation to a Lindblad equation valid also in the intermediate time regime (3.32) proceeds by ''symmetrization'' of the matrix elements of the Redfield relaxation operator, i.e., the right-hand side of Eq. (3.25). To this end we split the susceptibility in Eq. (3.25) as follows. In the first term we set

$$\chi''_+(\vec{k},\omega_{\mu\nu}-\vec{v}_p\cdot\vec{k}) \Rightarrow[(\chi''_+(\vec{k},\omega_{\mu\nu}-\vec{v}_p\cdot\vec{k}))(\chi''_+(\vec{k},\omega_{\alpha\nu}-\vec{v}_p\cdot\vec{k}))]^{1/2}, \tag{3.33a}$$

in the second term

$$\chi''_+(\vec{k},\omega_{\nu\mu}-\vec{v}_p\cdot\vec{k}) \Rightarrow[(\chi''_+(\vec{k},\omega_{\nu\mu}-\vec{v}_p\cdot\vec{k}))(\chi''_+(\vec{k},\omega_{\beta\mu}-\vec{v}_p\cdot\vec{k}))]^{1/2}, \tag{3.33b}$$

and in the third term

$$\chi''_+(\vec{k},\omega_{\nu\alpha}-\vec{v}_p\cdot\vec{k}) \simeq\chi''_+(\vec{k},\omega_{\mu\beta}-\vec{v}_p\cdot\vec{k}) \Rightarrow[(\chi''_+(\vec{k},\omega_{\nu\alpha}-\vec{v}_p\cdot\vec{k}))(\chi''_+(\vec{k},\omega_{\mu\beta}-\vec{v}_p\cdot\vec{k}))]^{1/2}. \tag{3.33c}$$

This construction in terms of square roots of χ''_+ is well defined because of the positive definiteness of the positive-frequency dissipative component of the susceptibility [Eq. (3.24)]. For those matrix elements that are nonzero within the secular approximation, Eqs. (3.33) agree with the result of the secular approximation. With this trick, we can now define transition operators S and $S^\dagger$ appearing in Lindblad relaxation operator (2.6) in terms of matrix elements in the energy eigenbasis as

$$S_{\alpha\beta}(\vec{k})=f(\vec{k})W_{\alpha\beta}(\vec{k})(2\chi''_+(\vec{k},\omega_{\beta\alpha}-\vec{k}\cdot\vec{v}_p))^{1/2}, \tag{3.34a}$$

$$S^\dagger_{\alpha\beta}(\vec{k})=f^*(\vec{k})W^\dagger_{\alpha\beta}(\vec{k})[2\chi''_+(\vec{k},-(\omega_{\beta\alpha}+\vec{k}\cdot\vec{v}_p))]^{1/2} \tag{3.34b}$$

$$=f^*(\vec{k})W^\dagger_{\alpha\beta}(\vec{k})(2\chi''_+(\vec{k},\omega_{\alpha\beta}-\vec{k}\vec{v}_p))^{1/2}. \tag{3.34c}$$

Inserting Eqs. (3.33) and (3.34) into Eq. (3.25) results in a quantum master equation with the relaxation superoperator $R^{(L)}$ in the Lindblad form (2.6). This result represents a novel generalization of the secular approximation which remains valid at time scales $t\leqslant t_I$. We will illustrate its utility below after calculating the relaxation operator for different environmental interactions explicitly.

IV. CALCULATION OF THE RELAXATION SUPEROPERATOR

In this section we analyze the properties of the Lindblad relaxation superoperator $R^{(L)}$, Eq, (2.6), as determined by the transition operators S and $S^\dagger$ in Eq. (3.34). We consider the interaction of the internal electronic state of an ion with three different environments: the radiation field $\mathbf{V}^{(r)}_{SR}$ the quasi-free-electrons of the solid $\mathbf{V}^{(ee)}_{SR}$, and the ionic cores of the solid $\mathbf{V}^{(c)}_{SR}$. We emphasize similarities and differences between the different relaxation channels. We perform independent numerical simulations for Kr^{35+} ions with a velocity $v_p=47$ a.u. interacting with either environment. We use time t and propagation length in the laboratory frame, d, interchangeably, since $d=v_pt$ and v_p can be treated as a constant. The latter takes into account that the slowing down of the ion at high collision velocities, v_p, and for thin foils can be safely neglected. The zero-point $t=0(d=0)$ corresponds to the time at which the ion enters the foil.

We also analyze the structural differences between the (inverse) lifetimes and the diagonal elements of Γ. If the system is initially in a pure state $|\alpha\rangle$ with a population $\sigma_{\alpha\alpha}=1$, the coupling to the reservoir yields [see Eq. (3.26)] an exponential damping $\sigma_{\alpha\alpha}=\exp(-t/\tau_\alpha)$, where the inverse lifetime τ^{-1}_α is defined by

$$\tau^{-1}_\alpha\equiv-R_{\alpha\alpha\alpha\alpha}=\Gamma_{\alpha\alpha}-\frac{1}{V}\sum_{\vec{k}}|S_{\alpha\alpha}(\vec{k})|^2. \tag{4.1}$$

The last term on the rhs of Eq. (4.1) subtracts from $\Gamma_{\alpha\alpha}$ the contribution involving transitions from $|\alpha\rangle$ to $|\alpha\rangle$. Therefore, τ^{-1}_α and $\Gamma_{\alpha\alpha}$ are, depending on the interaction with the environment, in general substantially different. Expressed in terms of propagation distance, the population $\sigma_{\alpha\alpha}$ decays exponentially as $\sigma_{\alpha\alpha}=\exp(-d/d_\alpha)$, where the decay length d_α is given by

$$d_\alpha=v_p\tau_\alpha. \tag{4.2}$$

A. Radiation field

The interaction with the vacuum fluctuations of the radiation field is a subject well studied in the context of photon-

atom interactions and quantum optics [30,32]. We only briefly review the essential ingredients to highlight the similarities and differences to collisional relaxation for which detailed studies appear to be missing. As usual, the radiation field is described in terms of a set of operators $\{\mathfrak{b}_\lambda^\dagger(\vec{k})\}$ and $\{\mathfrak{b}_\lambda(\vec{k})\}$, which are the creation and annihilation operators of a photon with wave-vector $\vec{k}$ and polarization $\hat{e}_{\hat{k},\lambda}$, where $\hat{k}=\vec{k}/k$ and $\hat{k}\cdot\hat{e}_{\hat{k},\lambda}=0$. The interaction operator for the coupling to the radiation field in the Coulomb gauge is given by

$$\begin{aligned}\mathbf{V}_{SR}^{(r)}(\vec{r},\{\mathfrak{b}_\lambda(\vec{k})\}) &= \frac{i}{c}\vec{\mathbf{A}}\cdot\vec{\nabla}_r \\ &= \sqrt{\frac{2\pi}{V}}\sum_{\vec{k},\lambda}\frac{[\hat{e}_{-\hat{k},\lambda}\mathfrak{b}_\lambda(-\vec{k})+\hat{e}_{\hat{k},\lambda}\mathfrak{b}_\lambda^\dagger(\vec{k})]}{\sqrt{ck}}(ie^{-i\vec{k}\cdot\vec{r}}\vec{\nabla}_r),\end{aligned} \tag{4.3}$$

where $\vec{r}=(r_1,r_2,r_3)=\Sigma_{\mathfrak{z}=1}^3 r_\mathfrak{z}\hat{e}_\mathfrak{z}$ is the coordinate of the electron in a frame of reference moving with the ion and $\vec{\mathbf{A}}(\vec{r})$ is the vector potential of the radiation field. Clearly, the interaction potential can be factorized as in Eq. (3.8). However, in order to simplify the problem, we perform the dipole approximation [we replace $\exp(-i\vec{k}\cdot\vec{r})\simeq 1$], which reduces the interaction to a much simpler factorization

$$\mathbf{V}_{SR}^{(r)}(\vec{r},\{\mathfrak{b}_\lambda(\vec{k})\})\simeq\frac{i}{c}\vec{\mathcal{A}}^D\cdot\vec{\nabla}_r=\frac{i}{c}\sum_{\mathfrak{z}=1}^3\mathcal{A}_\mathfrak{z}^D\frac{d}{dr_\mathfrak{z}}, \tag{4.4}$$

where $\vec{\mathcal{A}}^D$ is the dipole form of the vector potential, which only acts on the reservoir degrees of freedom. This decomposition allows us to identify the ingredients in Eq. (3.8) as the scalar $f(\mathfrak{z})=1$, the operators $W(\mathfrak{z})=id/dr_\mathfrak{z}$, and

$$\mathcal{B}^\dagger(\mathfrak{z})=\frac{\mathcal{A}_\mathfrak{z}^D}{c}=\hat{e}_\mathfrak{z}\sqrt{\frac{2\pi}{V}}\sum_{\vec{k},\lambda}\frac{[\hat{e}_{-\hat{k},\lambda}\mathfrak{b}_\lambda(-\vec{k})+\hat{e}_{\hat{k},\lambda}\mathfrak{b}_\lambda^\dagger(\vec{k})]}{\sqrt{ck}}. \tag{4.5}$$

The resulting susceptibility is

$$\chi_+^{(r)\prime\prime}(\mathfrak{z},\omega)=\chi_+^{(r)\prime\prime}(\omega)=\frac{\omega}{(2\pi c)^3}\theta(\omega), \tag{4.6}$$

which is isotropic. The susceptibility increases with ω without bound (which reflects well-known divergences in QED). In the present context, the key observation is that the ω spectrum is sufficiently broad and the correlation time τ_c sufficiently short ($\tau_c\to 0$) so that the Markov approximation can be safely applied.

Susceptibility (4.6) determines, employing Eq. (3.34), the jump operators entering the Lindblad relaxation operator for radiative decay,

$$R^{(L,r)}\sigma=-\frac{1}{2}\sum_{\mathfrak{z}=1}^3[S^{(r)\dagger}(\mathfrak{z})S^{(r)}(\mathfrak{z})\sigma+\sigma S^{(r)\dagger}(\mathfrak{z})S^{(r)}(\mathfrak{z}) -2S^{(r)}(\mathfrak{z})\sigma S^{(r)\dagger}(\mathfrak{z})], \tag{4.7}$$

where, using $\langle\alpha|\vec{\nabla}_r|\beta\rangle=-\omega_{\alpha\beta}\langle\alpha|\vec{r}|\beta\rangle$,

$$S_{\alpha\beta}^{(r)}(\mathfrak{z})=\frac{2}{\sqrt{3c^3}}\omega_{\beta\alpha}^{3/2}\langle\alpha|r_\mathfrak{z}|\beta\rangle\theta(\omega_{\beta\alpha}). \tag{4.8}$$

The corresponding decay operator, Eq. (2.14), for the radiation field becomes

$$\Gamma_{\alpha\beta}^{(r)}=\sum_{\nu,\mathfrak{z}}S_{\alpha\nu}^{(r)\dagger}(\mathfrak{z})S_{\nu\beta}^{(r)}(\mathfrak{z})=\frac{4}{3c^3}\sum_{\nu,\mathfrak{z}}\omega_{\alpha\nu}^{3/2}\omega_{\beta\nu}^{3/2}\langle\alpha|r_\mathfrak{z}|\nu\rangle \times\langle\nu|r_\mathfrak{z}|\beta\rangle. \tag{4.9}$$

And the inverse lifetime [Eq. (4.1)] of a given state $|\alpha\rangle$ adopts the well-known form of the Einstein A coefficient

$$(\tau_\alpha^{(r)})^{-1}=\Gamma_{\alpha\alpha}^{(r)}=\sum_\nu\frac{4\omega_{\alpha\nu}^3}{3c^3}|\langle\alpha|\vec{r}|\nu\rangle|^2. \tag{4.10}$$

For radiative decay τ_α^{-1} and $\Gamma_{\alpha\alpha}$ agree because $\alpha\to\alpha$ transitions are absent for photon emission.

The physics described by the present Lindblad relaxation operator is illustrated in Figs. 1, 2, and 3. Figure 1 displays density plots of the relative coherences

$$Q_{\alpha\beta}=\frac{|\sigma_{\alpha\beta}|}{\sqrt{\sigma_{\alpha\alpha}\sigma_{\beta\beta}}} \tag{4.11}$$

in the α-β plane (for $\sigma_{\alpha\alpha}<10^{-10}$ or $\sigma_{\beta\beta}<10^{-10}$ we set $Q_{\alpha\beta}=0$). Since density matrices have the property $|\sigma_{\alpha\beta}|\leqslant\sqrt{\sigma_{\alpha\alpha}\sigma_{\beta\beta}}$, the relative coherence takes values in the interval $0<Q_{\alpha\beta}<1$. Note that all diagonal elements $Q_{\alpha\alpha}$ are equal to unity (unless $\sigma_{\alpha\alpha}<10^{-10}$), and, therefore, the figure does not provide a quantitative measure of the time evolution for populations. If the system is in a pure state, all off-diagonal relative coherences of populated states are equal to unity. Finite relative coherences smaller than unity imply that the system is in a partially coherent state.

For the simulation in this section we use as system Hamiltonian that of the hydrogenic ion in vacuum,

$$H_S^{(v)}\equiv-\frac{\nabla_{\vec{r}}^2}{2}-\frac{Z_p}{r}+\Delta H_{rel}, \tag{4.12}$$

where ΔH_{rel} represents relativistic and Lamb shift corrections [4], which will also enter the full simulation when we calculate the post-foil evolution. The indices α, β of the relative coherences refer here to the eigenstates $|\alpha\rangle$ and $|\beta\rangle$ of the system Hamiltonian (4.12) and can be expressed as $|\alpha\rangle=|nljm_j\rangle$, where n is the principal quantum number, l is the orbital angular momentum, and j and m_j are the total angular momentum and its projection onto the z axis. In Fig. 1 we consider a Kr^{35+} ($Z_p=36$) initially in the pure hydro-

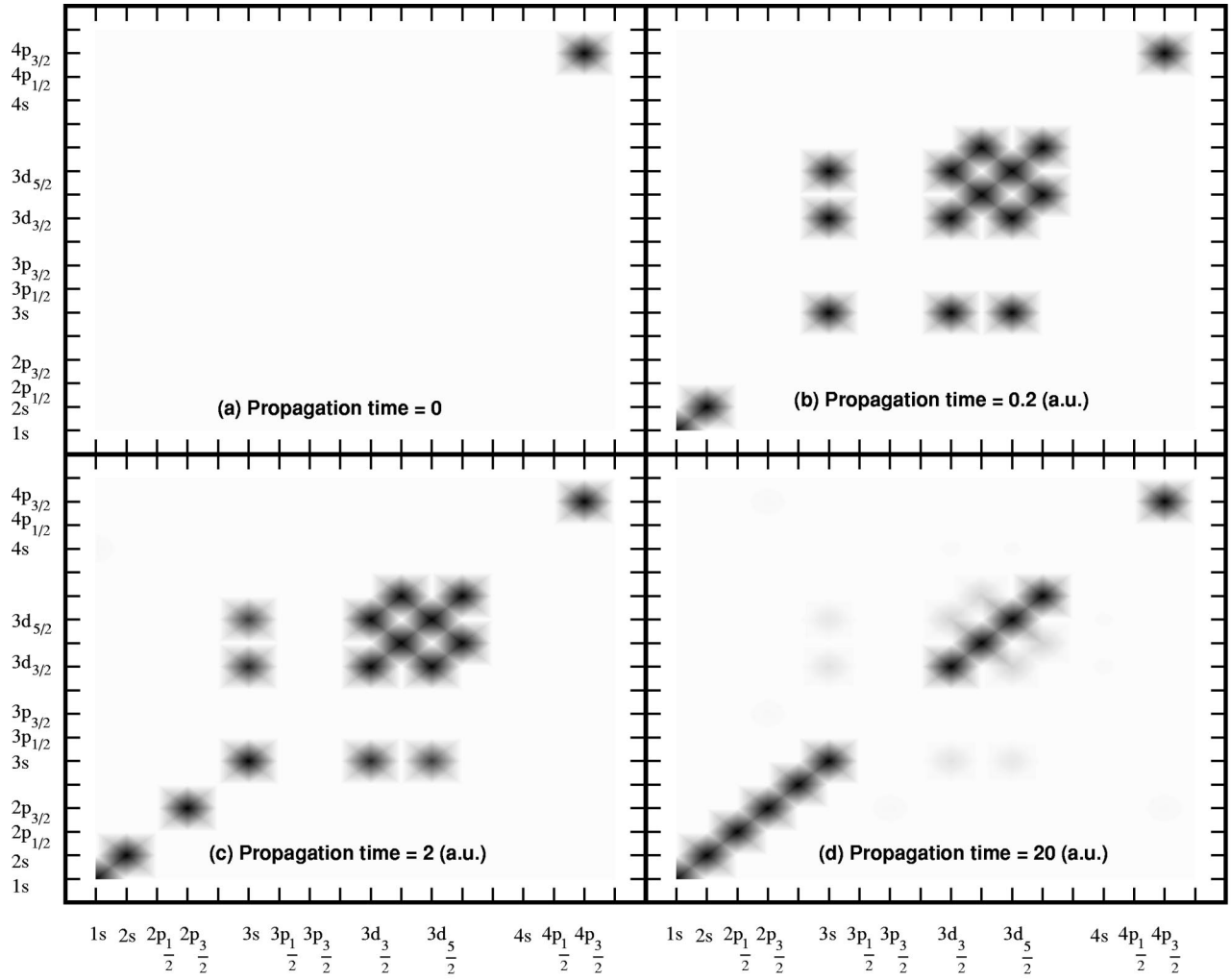

FIG. 1. Density plots of relative coherences of the reduced density matrix of a Kr^{35+} ion that radiatively decays for various propagation times as a function of the state index. The system is initially prepared in the pure state $|\psi(0)\rangle = |4p_{3/2,1/2}\rangle$ (only $m_j > 0$ states are shown for clarity).

genic state $|\Psi(0)\rangle = |4p_{3/2,1/2}\rangle$, which is subject only to spontaneous decay due to the interaction with the radiation field. Direct decay channels are the $1s$, $2s$, $3s$, and $3d$ states ($4p \rightarrow 2p$ and $4p \rightarrow 3p$ transitions are dipole forbidden but the $2p$ levels are populated slowly and indirectly via the decay of the $3s$ or $3d$ states). A remarkable aspect of the radiative decay from the initial state is that, unless a measurement is taken, i.e., the wave function is projected onto eigenstates of observables (e.g., photon energy), the system decays into a coherent superposition of states. Intershell coherences (different n quantum numbers) are rapidly washed out as a consequence of their large level splitting $\omega_{\alpha\beta}$ (i.e., the decoherence time due to dephasing $t_I = 2\pi/|\omega_{\alpha\beta}|$ [Eq. (3.32)] is very small). Therefore, in the following we focus on the intrashell coherences. The most striking feature in Fig. 1 is the transient buildup of off-diagonal elements ($3s$-$3d$ and $3d$-$3d$ coherences) at short times $t < t_I$ and their successive decay at much longer times $t \gg t_I$. Such features are absent in the standard Lindblad form based on secular approximation (3.28).

In order to verify the accuracy of the proposed jump operators [Eqs. (3.34) and (4.8)] entering the Lindblad form, we compare in Fig. 2 the time evolution of selected density-matrix elements with the result obtained solving the full Redfield equation (3.25) as well as that of the Lindblad equations using the standard secular approximation [31,33]. For the diagonal elements describing the population of the $3s_{1/2,-1/2}$ and $3d_{3/2,-1/2}$ states all three approximations agree well with each other. However, only our Lindblad form can reproduce the transient buildup of coherence due to the spontaneous decay as predicted by the Redfield equation. The secular approximation, by construction, fails. Coherences begin to be damped out for times $t > t_I = 2\pi/|\omega_{3s,3d}| = 7.6$ a.u. Nevertheless, smaller nonvanishing coherences can still be observed even beyond t_I, the reason being that the radiative lifetime of the ''feeder'' state $\tau^{(r)}_{4p_{3/2}} = 286$ a.u. is even longer and this state continuously replenishes the coherence. The point to be noted is that the standard secular approximation, therefore, fails even for times longer than t_I and up to the lifetime of the feeder state $\tau^{(r)}_{4p_{3/2}}$. It is thus completely inadequate for the entire transient regime. In Fig. 3 we provide another

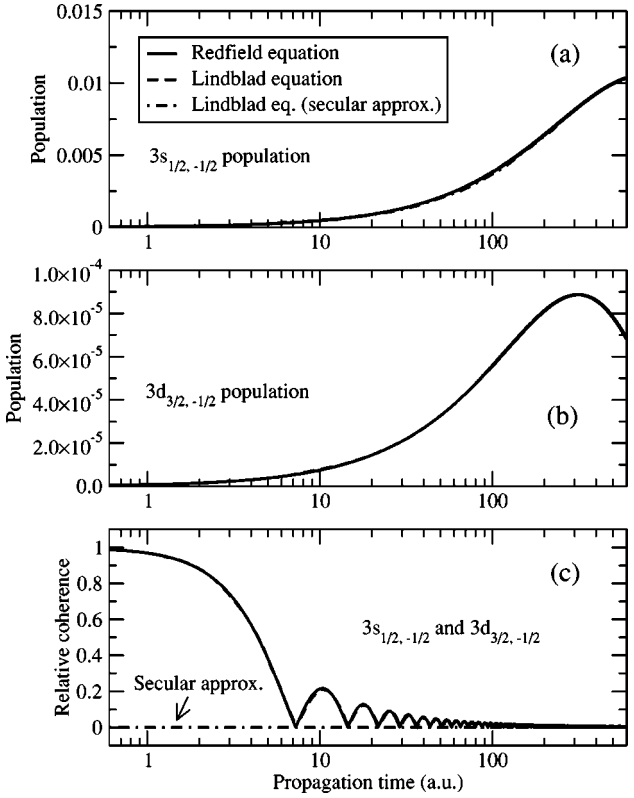

FIG. 2. Comparison of selected elements of the reduced density matrix of a Kr^{35+} ion that radiatively decays calculated using three different approximations: Redfield equation, Lindblad equation in secular approximation and in the present approximation. The system is initially prepared in the pure state $|\psi(0)\rangle = |4p_{3/2,1/2}\rangle$. (a) The population of the $3s_{1/2,-1/2}$ state, (b) the population of the $3d_{3/2,-1/2}$ state, and (c) the relative coherence between the $3s_{1/2,-1/2}$ and $3d_{3/2,-1/2}$ states.

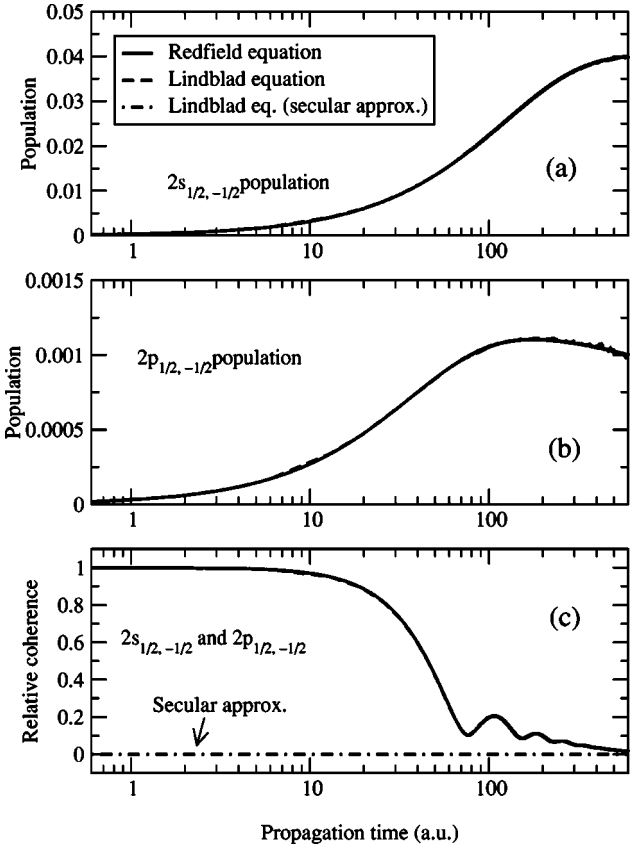

FIG. 3. Comparison of selected elements of the reduced density matrix of a Kr^{35+} ion that radiatively decays calculated using three different approximations (as in Fig. 2). The system is initially prepared in the pure state $|\psi(0)\rangle = (|3s_{1/2,-1/2}\rangle + |3p_{1/2,-1/2}\rangle)/\sqrt{2}$. (a) The population of the $2s_{1/2,-1/2}$ state, (b) the population of the $2p_{1/2,-1/2}$ state, and (c) the relative coherence between the $2s_{1/2,-1/2}$ and $2p_{1/2,-1/2}$ states.

example of coherent radiative decay for which the system is initially prepared in a coherent superposition of the $3s_{1/2,-1/2}$ and $3p_{1/2,-1/2}$ states: $|\Psi(0)\rangle = (|3s_{1/2,-1/2}\rangle + |3p_{1/2,-1/2}\rangle)/\sqrt{2}$ and we analyze the time evolution of the $2s_{1/2,-1/2}$ and $2p_{1/2,-1/2}$ states and their coherence. In this case, the coherence is damped due to the Lamb shift splitting yielding a longer dephasing decoherence time $t_I = 99$ a.u. However, also in this case the radiative lifetimes of the feeder states $\tau^{(r)}_{3p_{1/2}} = 123$ a.u. and $\tau^{(r)}_{3s_{1/2}} = 3844$ a.u. are longer than t_I, as in the previous case. Thus, similar conclusions can be drawn concerning the time needed for the secular approximation to hold.

B. Interaction with quasifree electrons of the solid

Consider now the interaction of an ion moving with respect to a free-electron gas with velocity $\vec{v}_p$, to be taken as the quantization axis (i.e., z-axis $\|\vec{v}_p$). The free-electron gas can be described through an ensemble of N_e electrons with number density $n_e = N_e/V$ with coordinates $\{\vec{\mathfrak{r}}'_i\}$ (we use primes for coordinates in the laboratory frame). The interaction of the projectile electron with the electrons in the solid is time dependent and is given by

$$\mathbf{V}^{(ee)}_{SR}(\vec{r},\{\vec{\mathfrak{r}}'_i\},t) = \sum_{i=1}^{N_e} \frac{1}{|\vec{\mathfrak{r}}'_i - \vec{v}_p t - \vec{r}|} = \int d^3x \int d^3x' \frac{\rho_e(\vec{x}')\rho_p(\vec{x})}{|\vec{x}' - \vec{v}_p t - \vec{x}|}, \quad (4.13)$$

where the pointlike charge densities are given by

$$\rho_p(\vec{x}) = \delta(\vec{x} - \vec{r}), \quad \rho_e(\vec{x}') = \sum_{i=1}^{N_e} \delta(\vec{x}' - \vec{\mathfrak{r}}'_i). \quad (4.14)$$

In order to express the interaction as in Eq. (3.8), we introduce the Fourier transforms of the charge densities

$$\tilde{\rho}_p(\vec{k}) = e^{i\vec{k}\cdot\vec{r}}, \quad \tilde{\rho}_e(\vec{k}) = \sum_{i=1}^{N_e} e^{i\vec{k}\cdot\vec{\mathfrak{r}}'_i} \quad (4.15)$$

Using the fact that $\int d^3x \, \exp(i\vec{x}\cdot\vec{k})(1/x) = 4\pi/k^2$, the interaction can be rewritten as

$$V_{SR}^{(ee)}(\vec{r},\{\vec{r}_i'\},t)=\frac{1}{V}\sum_{\vec{k}}\ \frac{4\pi}{k^2}e^{i\vec{k}\cdot\vec{v}_p t}\tilde{\rho}_p(\vec{k})\tilde{\rho}_e^{\dagger}(\vec{k}), \tag{4.16}$$

which is of the form of Eq. (3.8) with the substitutions $\mathcal{B}(\vec{k})=\tilde{\rho}_e(\vec{k})$, $W(\hat{k})=\tilde{\rho}_p(\vec{k})$, and $f(\vec{k})=4\pi/k^2$. Accordingly, the relevant reservoir Green's function (3.10) in the present case is related to the density-density correlation function and the corresponding susceptibility reads [35]

$$\chi_+^{(ee)\prime\prime}(\vec{k},\omega)=\pi\sum_n\ |\{0|\tilde{\rho}_e^{\dagger}(\vec{k})|n\}|^2\delta(\omega-\Omega_{n0}). \tag{4.17}$$

The latter is directly related to the inverse dielectric function as

$$\theta(\omega)\mathrm{Im}\left(\frac{-1}{\epsilon(\vec{k},\omega)}\right)=\frac{4\pi}{k^2}\chi_+^{(ee)\prime\prime}(\vec{k},\omega), \tag{4.18}$$

where the prefactor to the rhs is the Fourier transform of the Coulomb interaction and coincides with $f(\vec{k})$. Equation (4.18) allows us to use dielectric functions in parametrized forms [13,36] for realistic systems, as obtained from experimental data from photon absorption and electron energy-loss spectroscopy. With such a choice, $\mathrm{Im}(-1/\epsilon)$ includes all electronic excitations of the target including those of inner shells and not just those of the valence band.

Using Eq. (3.34), the jump operator representing scattering of the projectile electron at target electrons as reservoir is given by

$$S_{\alpha\beta}^{(ee)}(\vec{k})=\frac{\sqrt{8\pi}}{k}\left[\mathrm{Im}\left(\frac{-1}{\epsilon(\vec{k},\omega_{\beta\alpha}-\vec{k}\cdot\vec{v}_p)}\right)\right]^{1/2}\langle\alpha|e^{i\vec{k}\cdot\vec{r}}|\beta\rangle \times\theta(\omega_{\beta\alpha}-\vec{k}\cdot\vec{v}_p). \tag{4.19}$$

Upon converting the Fourier sum into an integral (i.e., $V^{-1}\Sigma_k=(2\pi)^{-3}\int d^3k$), the Lindblad relaxation operator for electron-electron scattering $R^{(L,ee)}$ becomes

$$R^{(L,ee)}\sigma=-\frac{1}{16\pi^3}\int d^3k[S^{(ee)\dagger}(\vec{k})S^{(ee)}(\vec{k})\sigma +\sigma S^{(ee)\dagger}(\vec{k})S^{(ee)}(\vec{k})-2S^{(ee)}(\vec{k})\sigma S^{(ee)\dagger}(\vec{k})]. \tag{4.20}$$

One of the basic ingredients of the jump operator for the present case is given by the form factor $\langle\alpha|e^{i\vec{k}\vec{r}}|\beta\rangle$, which represents a transition induced by a momentum transfer $\vec{k}$ (i.e., a boost in momentum). The step function in Eq. (4.19) provides a restriction on the values of momentum transfers that can be delivered to the electron,

$$k_z\leqslant k_z^{max}\equiv\frac{\omega_{\beta\alpha}}{v_p}. \tag{4.21}$$

This restriction on the integration domain over $\vec{k}$ expresses the fact that the effective environment consists not just of the electron gas in its ground state but includes the motion of the projectile relative to the electron gas with velocity v_p, which leads to a Doppler shift of the frequency spectrum of the susceptibility χ_+'' [or $\mathrm{Im}(-1/\epsilon)$]. The motion serves as the heat bath that drives inelastic transitions.

For endothermic reactions ($\omega_{\beta\alpha}<0$), Eq. (4.21) implies the momentum transfer to be antiparallel to the projectile velocity. The jump operator Eq. (4.20) depends on three independent variables, namely, $k=\sqrt{k_x^2+k_y^2+k_z^2}$, $\phi_k=\tan^{-1}(k_y/k_x)$, and k_z. In this case, the integration domain of the corresponding relaxation operator is given by $0<\phi_k<2\pi$, $k>k_{min}=|k_z^{max}|\equiv|\omega_{\beta\alpha}|/v_p$, where k_{min} is usually referred as the minimum momentum transfer and, up to a sign, agrees with the constraint Eq. (4.21).

Matrix elements of the decay operator for *e*-*e* scattering are given by

$$\Gamma_{\alpha\beta}^{(ee)}=\int\ \frac{d^3k}{\pi^2k^2}\sum_\nu\ \langle\alpha|e^{-i\vec{k}\cdot\vec{r}}|\nu\rangle\langle\nu|e^{i\vec{k}\cdot\vec{r}}|\beta\rangle \times\theta(\omega_{\beta\nu}-\vec{k}\cdot\vec{v}_p)\,\theta(\omega_{\alpha\nu}-\vec{k}\cdot\vec{v}_p) \times\left[\mathrm{Im}\left(\frac{-1}{\epsilon(\vec{k},\omega_{\alpha\nu}-\vec{k}\cdot\vec{v}_p)}\right)\mathrm{Im}\left(\frac{-1}{\epsilon(\vec{k},\omega_{\beta\nu}-\vec{k}\cdot\vec{v}_p)}\right)\right]^{1/2}. \tag{4.22}$$

The decay matrix for *e*-*e* scattering is approximately diagonal in the unperturbed energy eigenbasis of the internal electronic state of the projectile (the same applies to electron-core scattering discussed below). This is due to the fact that the integrand in Eq. (4.22) places the dominant weight at small k and for $\alpha\rightarrow\alpha$ transitions $k_{min}=0$. For small values of k the boost can be expanded as

$$\langle\nu|e^{i\vec{k}\cdot\vec{r}}|\alpha\rangle=\delta_{\nu\alpha}+i\vec{k}\langle\nu|\vec{r}|\alpha\rangle+\mathcal{O}(k^2). \tag{4.23}$$

For diagonal elements [$\alpha=\beta$ in Eq. (4.22)], the first term of Eq. (4.23), $\delta_{\nu\alpha}$, describing elastic scattering without changing the internal state of the projectile electron dominates. (Here and in the following we refer to ''elastic processes'' as those processes for which the energy of the internal state of the projectile remains unchanged). In other words, elastic scattering, which does not represent decay at all, dominates the decay matrix. The origin of this apparent paradox is obvious from Eq. (4.1): the inverse lifetimes differ from the diagonal matrix elements of Γ whenever $S_{\alpha\alpha}\neq 0$. For *e*-*e* interactions, $(\tau_\alpha^{(ee)})^{-1}\ll\Gamma_{\alpha\alpha}^{(ee)}$, where the inverse collisional lifetime is given by

$$(\tau_\alpha^{(ee)})^{-1}=\sum_{\nu\neq\alpha}\ \int\ \frac{d^3k}{\pi^2k^2}|\langle\nu|e^{i\vec{k}\cdot\vec{r}}|\alpha\rangle|^2 \times\mathrm{Im}\left(\frac{-1}{\epsilon(\vec{k},\omega_{\alpha\nu}-\vec{k}\cdot\vec{v}_p)}\right)\theta(\omega_{\beta\alpha}-\vec{k}\cdot\vec{v}_p). \tag{4.24}$$

This differs from radiative decay, where $(\tau_\alpha^{(r)})^{-1}=\Gamma_{\alpha\alpha}^{(r)}$. The reason for this difference is that the jump operator for the interaction with the electromagnetic field has vanishing diagonal elements [i.e., the prefactor $\omega_{\beta\alpha}^{3/2}$ in Eq. (4.8) vanishes for $\beta=\alpha$]. The lifetime $\tau_\alpha^{(ee)}$ determines the decay rate of a given state while $\Gamma_{\alpha\alpha}^{(ee)}$ determines the jump times t_j entering the QTMC simulation. The former determines the decay length $d_\alpha^{(ee)}=v_p\tau_\alpha^{(ee)}$ of a given state [Eq. (4.2)], whereas the latter determines the collisional mean-free-path $\lambda_\alpha^{(ee)}=v_p/\Gamma_{\alpha\alpha}^{(ee)}$ when the system is in state $|\alpha\rangle$. The fact that $\lambda_\alpha^{(ee)}\gg d_\alpha^{(ee)}$ implies that the transition probabilities per jump into states $\beta\neq\alpha$ are small.

The presence of elastic and near-elastic relaxation channels due to soft collisions has consequences in terms of damping in off-diagonal elements of the reduced density operator. Suppose that we consider the subset of the Lindblad equation involving only $\sigma_{\alpha\beta}$ neglecting all couplings to other elements,

$$\frac{d}{dt}\sigma_{\alpha\beta}(t)=-i\omega_{\alpha\beta}\sigma_{\alpha\beta}(t)+R_{\alpha\beta\alpha\beta}^{(ee)}\sigma_{\alpha\beta}(t), \quad (4.25)$$

whose solution is

$$\sigma_{\alpha\beta}(t)=\sigma_{\alpha\beta}(0)e^{-i\omega_{\alpha\beta}t}e^{-R_{\alpha\beta\alpha\beta}^{(ee)}t}. \quad (4.26)$$

Clearly, $R_{\alpha\beta\alpha\beta}^{(ee)}$ can be considered as a damping or phase diffusion coefficient from which we can define the collisional decoherence length

$$D_{\alpha\beta}^{(ee)}=v_pR_{\alpha\beta\alpha\beta}^{(ee)}. \quad (4.27)$$

In the elastic limit [see Eq. (4.23)], where $W_{\alpha\nu}(\vec{k})\propto\delta_{\alpha\nu}$,

$$R_{\alpha\beta\alpha\beta}^{(ee)}(k\to 0^+)\simeq\frac{1}{V}\sum_{\vec{k}\to 0}|f(\vec{k})|^2\chi_+^{(ee)\prime\prime}(\vec{k},-\vec{v}_p\cdot\vec{k})\times|W_{\alpha\alpha}(\vec{k})-W_{\beta\beta}(\vec{k})|^2. \quad (4.28)$$

While diagonal elements ($\alpha=\beta$) are unaffected by elastic scattering because of the complete compensation of sink and source terms, off-diagonal elements are effectively damped by elastic scattering. Such processes are of particular importance for charged-particle scattering because of the dominance of the soft collisions due to the long-range Coulomb tail. For short-range interaction potentials the damping rate is smaller but it is also present and gives rise to collisional dephasing and decoherence in neutral gases.

In order to study the dynamics induced by the relaxation operator for *e-e* collisions [Eq. (4.20)], we have performed simulations for Kr^{35+} ions with velocity $v_p=47$ a.u. subject only to *e-e* interactions and using the system Hamiltonian $H_S^{(v)}$ [Eq. (4.12)]. Results illustrating the time evolution of selected matrix elements of $\sigma(t)$ are depicted in Fig. 4 for an environment represented by a parametrized dielectric function of an amorphous carbon foil [36]. The initial state in this simulation at $t=0$ is the coherent superposition $|\Psi(0)\rangle=(|3s_{1/2,-1/2}\rangle+|3p_{1/2,-1/2}\rangle)/\sqrt{2}$ and the results are depicted as a function of the propagation length $d=v_pt$. Since inelastic transitions are relatively weak, we focus on the populations and relative coherences involving states within the $n=3$ shell, namely, $|\alpha\rangle=|3s_{1/2,-1/2}\rangle$, $|\beta\rangle=|3p_{1/2,-1/2}\rangle$, $|\mu\rangle=|3p_{3/2,-3/2}\rangle$, and $|\nu\rangle=|3p_{3/2,1/2}\rangle$. Even though for the range of propagation lengths depicted in the figure about 100 collisions take place, most of the probability stays in the $|\alpha\rangle$ and $|\beta\rangle$ feeder states. They decay approximately exponentially with a decay length that is different from either $d_\alpha^{(ee)}$ or $d_\beta^{(ee)}$ because of the coherent superposition in the initial state. The time evolution of the initially unpopulated states is, in turn, approximately given by $\sigma_{\mu\mu}(t)\simeq\text{const}\times[1-\exp(-d/d_\mu^{(ee)})]$, which describes the population of a decaying state coupled to a feeder state with a constant population. The results depicted in the figure do indeed obey this form and the decay lengths of the fit curves agree with $d_{3p_{3/2,-3/2}}^{(ee)}$ and $d_{3p_{3/2,1/2}}^{(ee)}$.

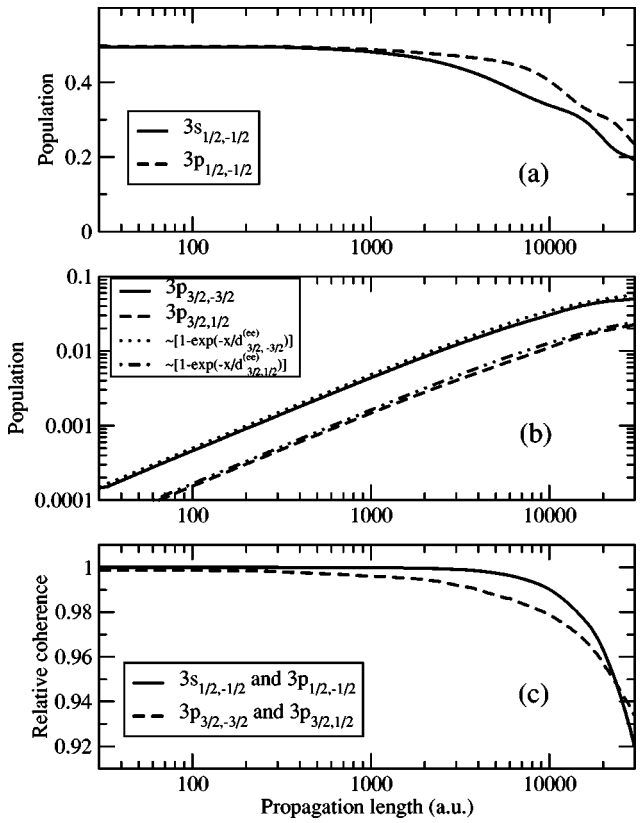

FIG. 4. Evolution of selected populations and coherences of the internal state of a Kr^{35+} ion moving with velocity $v_p=47$ a.u. subject to collisions with electrons in an amorphous carbon foil as a function of the propagation length. The system is initially prepared in the pure state $|\psi(0)\rangle=(|3s_{1/2,-1/2}\rangle+|3p_{1/2,-1/2}\rangle)/\sqrt{2}$. (a) The populations of the $3s_{1/2,-1/2}$ and $3p_{1/2,-1/2}$ states, (b) the populations of the $3p_{3/2,-3/2}$ and $3p_{3/2,1/2}$ states, and (c) the relative coherences between the $3s_{1/2,-1/2}$ and $3p_{1/2,-1/2}$ states and between the $3p_{3/2,-3/2}$ and $3p_{3/2,1/2}$ states.

In Fig. 4(c), the time evolution of the relative coherences $Q_{3s_{1/2,-1/2},3p_{1/2,-1/2}}$ and $Q_{3p_{3/2,-3/2},3p_{3/2,1/2}}$ is displayed. Due to

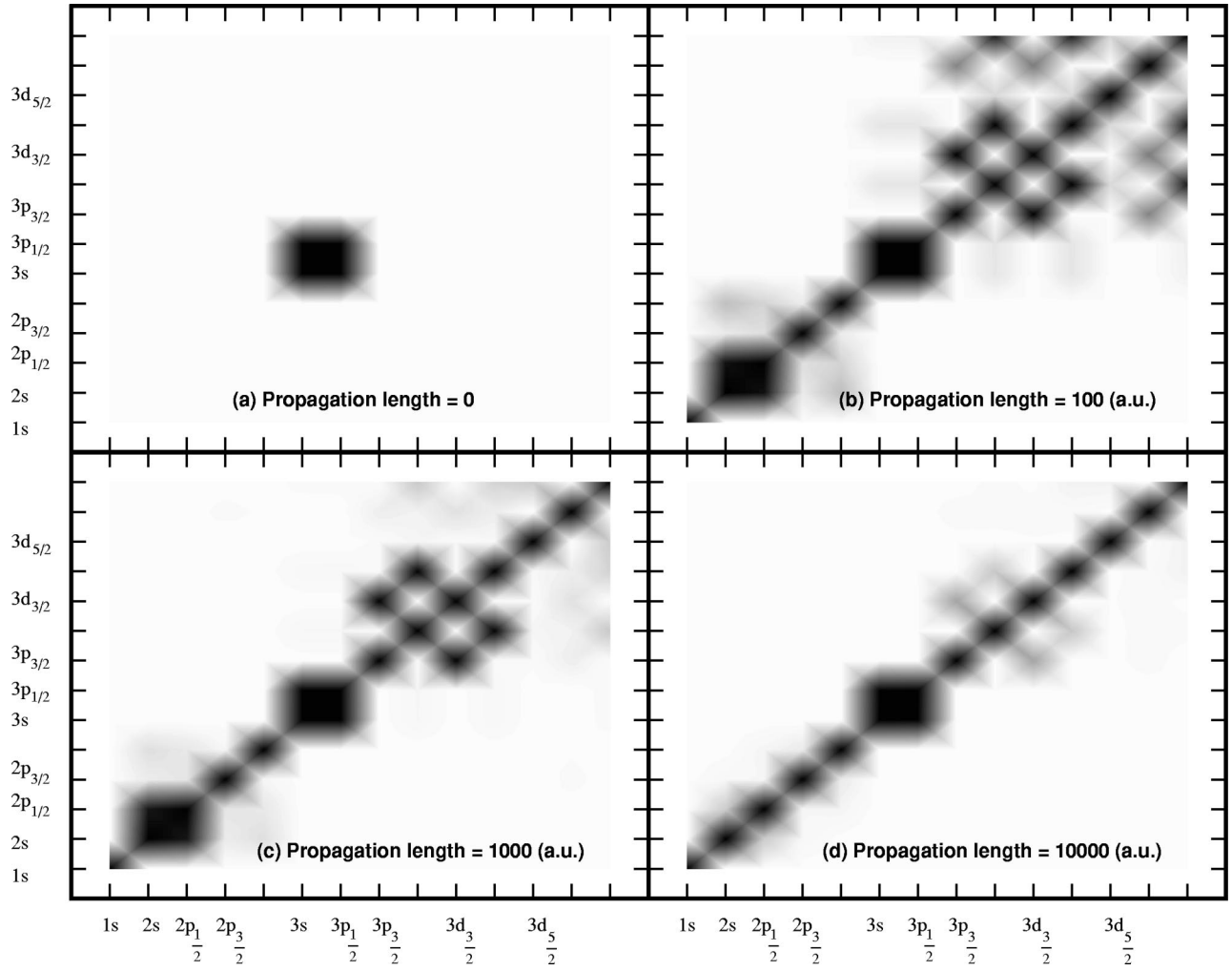

FIG. 5. Density plots of relative coherences of the reduced density matrix of the internal state of a Kr^{35+} ion moving with velocity $v_p=47$ a.u. subject to collisions with electrons in an amorphous carbon foil for various propagation lengths. The system is initially prepared in the pure state $|\psi(0)\rangle=(|3s_{1/2,-1/2}\rangle+|3p_{1/2,-1/2}\rangle)/\sqrt{2}$ (only matrix elements with $m_j<0$ are shown).

the initial conditions of this simulation, $Q_{3s_{1/2,-1/2},3p_{1/2,-1/2}}=1$ at $t=0$. With increasing propagation length, decay of this coherence sets in at $d\sim 10\,000$ a.u., which is close to the expected length of decoherence by dephasing ($d_I=t_I v_p=2\pi v_p/|\omega_{\alpha\beta}|=15\,500$ a.u.). Interestingly, $Q_{3p_{3/2,-3/2},3p_{3/2,1/2}}$ also starts very close to unity indicating that the states $3p_{3/2,-3/2}$ and $3p_{3/2,1/2}$ are coherently populated by a single collision. Since these two states are degenerate, decoherence in this case is only a consequence of successive multiple collisions. Although both coherences tend to decay with increasing propagation length, they remain high with values above 0.9. This results from the fact that the interaction with electrons in the solid both generates coherences between states and decoheres the internal state of the ion. We can observe this behavior in Fig. 5 in more detail, where the relative coherences $Q_{\alpha\beta}$ are displayed in the α-β plane. The first panel displays the initial state. In the second panel ($d=100$ a.u.), states with the same principal quantum numbers are coherently populated by a single collision. Despite the fact that relative coherences diminish in magnitude as the propagation length increases, the system remains partially coherent even for the longest propagation length analyzed (last panel).

C. Interactions with ionic cores of the solid

Consider now the interaction of the electron with an ensemble of screened ionic cores, which can be described through an ensemble of N_A atoms with number density $n_A=N_A/V$ with coordinates $\{\vec{\mathfrak{R}}_i'\}$ in the laboratory frame. This problem is closely related to that in the preceding section. For a neutral system the atomic density n_A is related to the electron density $n_e=Z_T n_A$, where Z_T is the nuclear charge of the atoms in the solid. In line with the discussion above, the relevant degree of freedom in the target is the heavy particle motion while electronic excitations in the core are already included in the e-e scattering term as described by $\mathrm{Im}(-1/\epsilon)$. The inelastic processes considered in the following are therefore excitations of phonons. The first obvious difference between the e-e interaction and the e-c interaction is that the effective two-body interaction V_c is not pure Coulombic. The total interaction potential is given by

$$\mathbf{V}_{SR}^{(c)}(\vec{r},\{\vec{\Re}_i'\},t)=\sum_{i=1}^{N_A} V_c(\vec{\Re}_i'-\vec{v}_p t-\vec{r})$$

$$=\int d^3x \int d^3x' \rho_c(\vec{x}')\rho_p(\vec{x})V_c(\vec{x}'-\vec{v}_p t-\vec{x})$$

$$=\frac{1}{V}\sum_{\vec{k}} \tilde{V}_c(\vec{k})e^{i\vec{k}\cdot\vec{v}_p t}\tilde{\rho}_p(\vec{k})\tilde{\rho}_c^{\dagger}(\vec{k}), \qquad (4.29)$$

where the pointlike charge density of the target cores and its Fourier transform are given by

$$\rho_c(\vec{x}')=\sum_{i=1}^{N_A}\delta(\vec{x}'-\vec{\Re}_i'), \quad \tilde{\rho}_c(\vec{k})=\sum_{i=1}^{N_A} e^{i\vec{k}\cdot\vec{\Re}_i'}. \qquad (4.30)$$

Clearly, Eq. (4.29) is of the form of Eq. (3.8) with the system operator $W(\vec{k})=\tilde{\rho}_p(\vec{k})$ being the same as for e-e interactions while the reservoir operator $\mathcal{B}(\vec{k})=\tilde{\rho}_c(\vec{k})$, and $f(\vec{k})=\tilde{V}_c(\vec{k})$. The interaction potential with ionic cores, V_c, corresponds to an attractive screened Coulomb interaction. A typical choice, which is used in this work, is $V_c(\vec{r})=-(Z_T/r)\exp(-r/a_{TF})$ with the Thomas-Fermi screening length $a_{TF}=0.885Z_T^{-1/3}$ and the Fourier transform $\tilde{V}_c(\vec{k})=-(4\pi Z_T)/(k^2+a_{TF}^{-2})$.

The susceptibility entering the relaxation operator refers now to the density fluctuation of ionic cores. For the phonon excitation spectrum we consider for simplicity the dispersion relation

$$\omega=\frac{k^2}{2M_c}, \qquad (4.31)$$

where M_c is the mass of the ionic cores. Neglecting collective excitations and phonon damping, a simple choice for the susceptibility that satisfies the f- (or Thomas-Kuhn) sum rule [35]

$$\int_0^{\infty} d\omega \frac{2M_c}{k^2}\omega\chi_+^{(c)\prime\prime}(\vec{k},\omega)=\pi n_A \qquad (4.32)$$

is given by

$$\chi_+^{(c)\prime\prime}(\vec{k},\omega)=\pi n_A \delta\left(\omega-\frac{k^2}{2M_c}\right). \qquad (4.33)$$

The fundamental differences to electron-electron scattering result from the properties of the phonon dispersion. Because of the large mass M_c, the δ function in Eq. (4.33) peaks close to $\omega\simeq 0$. Consequently, the imaginary part of the susceptibility for electron-ion core scattering is approximately given by

$$\chi_+^{(c)\prime\prime}(k,\omega=\omega_{\alpha\beta}-\vec{v}_p\cdot\vec{k})\simeq\pi n_A\delta(\omega_{\alpha\beta}-\vec{v}_p\cdot\vec{k}). \qquad (4.34)$$

The relaxation channel involving ionic cores of the solid is therefore often, somewhat misleadingly, referred to as ''elastic scattering'' even though it can drive inelastic excitations of the internal state of the projectile as efficiently as the electron-electron channel. The term elastic originates here from the small energy transfer to the target degrees of freedom (i.e., $\omega\simeq 0$). The energy required for inelastic processes originates, as above, from the translational degree of freedom of the projectile. In order to distinguish this scattering process from true elastic scattering we will refer to this relaxation channel as electron-ion-core (c) scattering.

The δ function in Eq. (4.34) fixes the z component of the momentum transfer to

$$k_z=k_z^{\beta\alpha}=\frac{\omega_{\beta\alpha}}{v_p}. \qquad (4.35)$$

and implies that the absolute magnitude of the momentum transfer must be $k>k_{min}\equiv|\omega_{\beta\alpha}|/v_p$.

The δ function in Eq. (4.34) allows one to carry out the integration over k_z such that the final form of $R^{(L,c)}$ involves only a two-dimensional integral over $\vec{k}_\perp=\vec{k}-k_z\hat{z}$,

$$R^{(L,c)}\sigma=-\frac{1}{16\pi^3}\int d^2k_\perp[S^{(c)\dagger}(\vec{k}_\perp)S^{(c)}(\vec{k}_\perp)\sigma$$

$$+\sigma S^{(c)\dagger}(\vec{k}_\perp)S^{(c)}(\vec{k}_\perp)-2S^{(c)}(\vec{k}_\perp)\sigma S^{(c)\dagger}(\vec{k}_\perp)], \qquad (4.36)$$

where the jump operator is given by

$$S_{\alpha\beta}^{(c)}(\vec{k}_\perp)=\left(\frac{2\pi n_A}{v_p}\right)^{1/2}\tilde{V}_c(\vec{k}_\perp+\hat{z}k_z^{\beta\alpha})\langle\alpha|e^{i(\vec{k}_\perp+\hat{z}k_z^{\beta\alpha})\vec{r}}|\beta\rangle. \qquad (4.37)$$

The resulting decay matrix becomes

$$\Gamma_{\alpha\beta}^{(c)}==\frac{n_A}{4\pi^2 v_p}\sum_\nu \int d^2k_\perp\langle\alpha|e^{-i(\vec{k}_\perp+\hat{z}k_z^{\alpha\nu})\vec{r}}|\nu\rangle$$

$$\times\langle\nu|e^{i(\vec{k}_\perp+\hat{z}k_z^{\beta\nu})\vec{r}}|\beta\rangle\tilde{V}_c^*(\vec{k}_\perp+\hat{z}k_z^{\alpha\nu})\tilde{V}_c(\vec{k}_\perp+\hat{z}k_z^{\beta\nu}), \qquad (4.38)$$

whereas the inverse collisional lifetime adopts the form

$$(\tau_\alpha^{(c)})^{-1}=\frac{n_A}{4\pi^2 v_p}\sum_{\nu\neq\alpha}\int d^2k_\perp|\tilde{V}_c(\vec{k}_\perp+\hat{z}k_z^{\nu\alpha})|^2$$

$$\times|\langle\alpha|e^{i(\vec{k}_\perp+\hat{z}k_z^{\nu\alpha})\vec{r}}|\nu\rangle|^2, \qquad (4.39)$$

which can be used to define the decay length of each state $d_\alpha^{(c)}=v_p\tau_\alpha^{(c)}$, as in Eq. (4.2).

In Figs. 6 and 7, we analyze the effect of the relaxation operator $R^{(L,c)}$ (4.36) for a Kr^{35+} ion with $v_p=47$ traversing an amorphous carbon foil. The initial internal state of the ion consists of a statistical incoherent superposition of the $1s_{1/2,-1/2}$ and $1s_{1/2,1/2}$ states, which mimics typical experimental initial conditions [4]. Since $1s$ states are deeply bound, feeding higher-energy levels through core collisions is a slow process. In fact, the decay length of the ground state

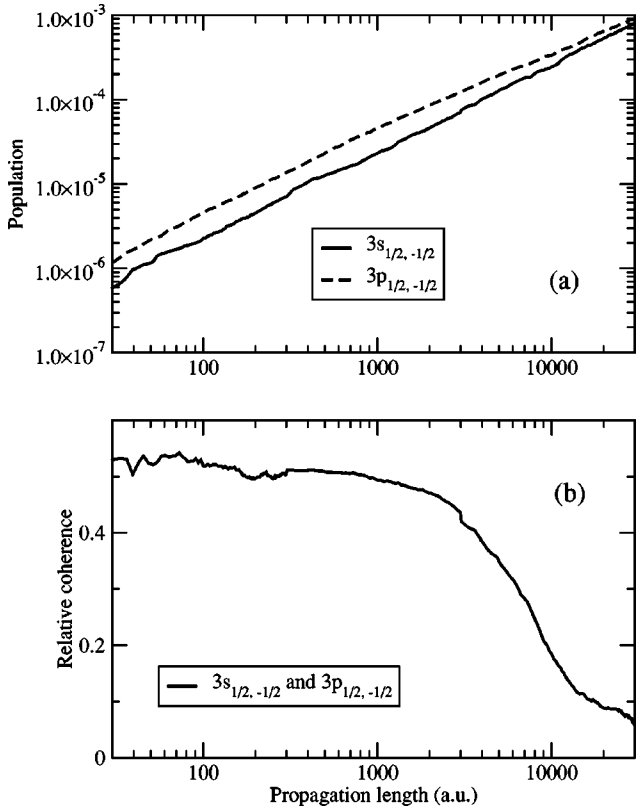

FIG. 6. Evolution of selected populations and coherences of the internal state of a Kr^{35+} ion moving with velocity $v_p=47$ a.u. subject to collisions with screened nuclei in an amorphous carbon foil as a function of the propagation length. The system is initially prepared in a statistical incoherent superposition of the $1s_{1/2,-1/2}$ and $1s_{1/2,1/2}$ states. (a) The populations of the $3s_{1/2,-1/2}$ and $3p_{1/2,-1/2}$ states and (b) the relative coherence between the $3s_{1/2,-1/2}$ and $3p_{1/2,-1/2}$ states.

is $d_{1s}^{(c)}\sim 8\times 10^5$, which is larger than the range of propagation length shown in Fig. 6 and much larger than the typical collisional mean-free path of free electrons $\lambda^{(c)}\sim 10^3$. We focus here on the evolution of the populations of the $3s_{1/2,-1/2}$ and $3p_{1/2,-1/2}$ states [Fig. 6(a)] and their relative coherence $Q_{3s_{1/2,-1/2},3p_{1/2,-1/2}}$ [Fig. 6(b)] as a function of the propagation length. Initially, the $3s_{1/2,-1/2}$ and $3p_{1/2,-1/2}$ states are not populated and, therefore, the populations increase at first as $\sigma_{\mu\mu}(t)\simeq \text{const}\times[1-\exp(-v_p t/d_\mu^{(c)})]$. The dominance of the excitation of p states is valid for all n shells and indicates that the typical momentum transfers involved in the excitation process are small such that the boost is near the dipole limit [see Eq. (4.23)]. The relative coherence in Fig. 6(b) at $d=0$ is $Q_{3s_{1/2,-1/2},3p_{1/2,-1/2}}\sim 0.5$ and, subsequently, it starts dropping rapidly from this value at $d\sim 3000$ a.u. This decay length is close to the collisional decoherence length [Eq. (4.27)] and is much shorter than the dephasing decoherence length of these states, $v_p t_I\sim 15\,500$ a.u. [see Eq. (3.32)]. In other words, the interaction with the atomic cores of the solid decoheres the internal state of the ion very efficiently. This trend can be seen directly in Fig. 7, where we display the relative coherence in state space. For short propagation lengths, states are coherently populated by a single collision. For long propagation lengths, however, coherences are almost completely washed out and the internal state of the ion turns into an incoherent mixture of states.

V. SIMULATION OF THE INTERNAL STATE EVOLUTION IN ION-SOLID INTERACTIONS

A. Implementation of the QTMC

In this section we combine the relaxation processes discussed in the preceding section for a fast hydrogenlike ion with nuclear charge Z_p and velocity v_p through an amorphous foil with a given thickness d. Accordingly, the coupling of the system, the internal electronic state of the projectile, to the environment, the solid and the electromagnetic field, is given by

$$\mathbf{V}_{SR}=\mathbf{V}_{SR}^{(r)}+\mathbf{V}_{SR}^{(ee)}+\mathbf{V}_{SR}^{(c)}. \tag{5.1}$$

Within linear response theory, the couplings to the various environmental degrees of freedom are independent of each other and are independent stochastic processes. Accordingly, the relaxation operator entering the Lindblad equation becomes

$$R^{(L)}=\sum_\ell R^{(L,\ell)}=R^{(L,r)}+R^{(L,ee)}+R^{(L,c)}, \tag{5.2}$$

where $\ell=r,ee,c$ denotes independent relaxation channels for radiative decay, electron-electron, and electron-core scattering. Thus, one can implement all the tools introduced in Sec. II provided that the index $\vec{k}$ [Eq. (2.6)] is replaced by appropriate indices for each environmental degree of freedom: $\jmath$ for $\ell=r$ [Eq. (4.7)], $\vec{k}$ for $\ell=ee$ [Eq. (4.20)], and $\vec{k}_\perp$ for $\ell=c$ [Eq. (4.36)].

The solution of the Lindblad equation for the relaxation operator in Eq. (5.2) by the QTMC method proceeds as follows. Between stochastic jumps, the continuous time evolution [Eq. (2.12)] is governed by an effective non-Hermitian Hamiltonian (2.13) with the total decay operator

$$\Gamma=\sum_\ell \Gamma^{(\ell)}=\Gamma^{(r)}+\Gamma^{(ee)}+\Gamma^{(c)}, \tag{5.3}$$

where the decay matrices for each relaxation channel are given by Eqs. (4.9), (4.22), and (4.38). The Hamiltonian H_S in Eq. (2.13) is assumed to contain all energy shifts due to the interaction between the system and the environmental degrees of freedom. The continuous evolution intertwines different relaxation channels. The stochastic times t_j are determined by the solution of the implicit Eq. (2.19), which incorporates the reduction in state population due to all possible relaxation channels. The probability for the occurrence of one particular relaxation channel (r, ee, or c) being responsible for the next jump is determined by

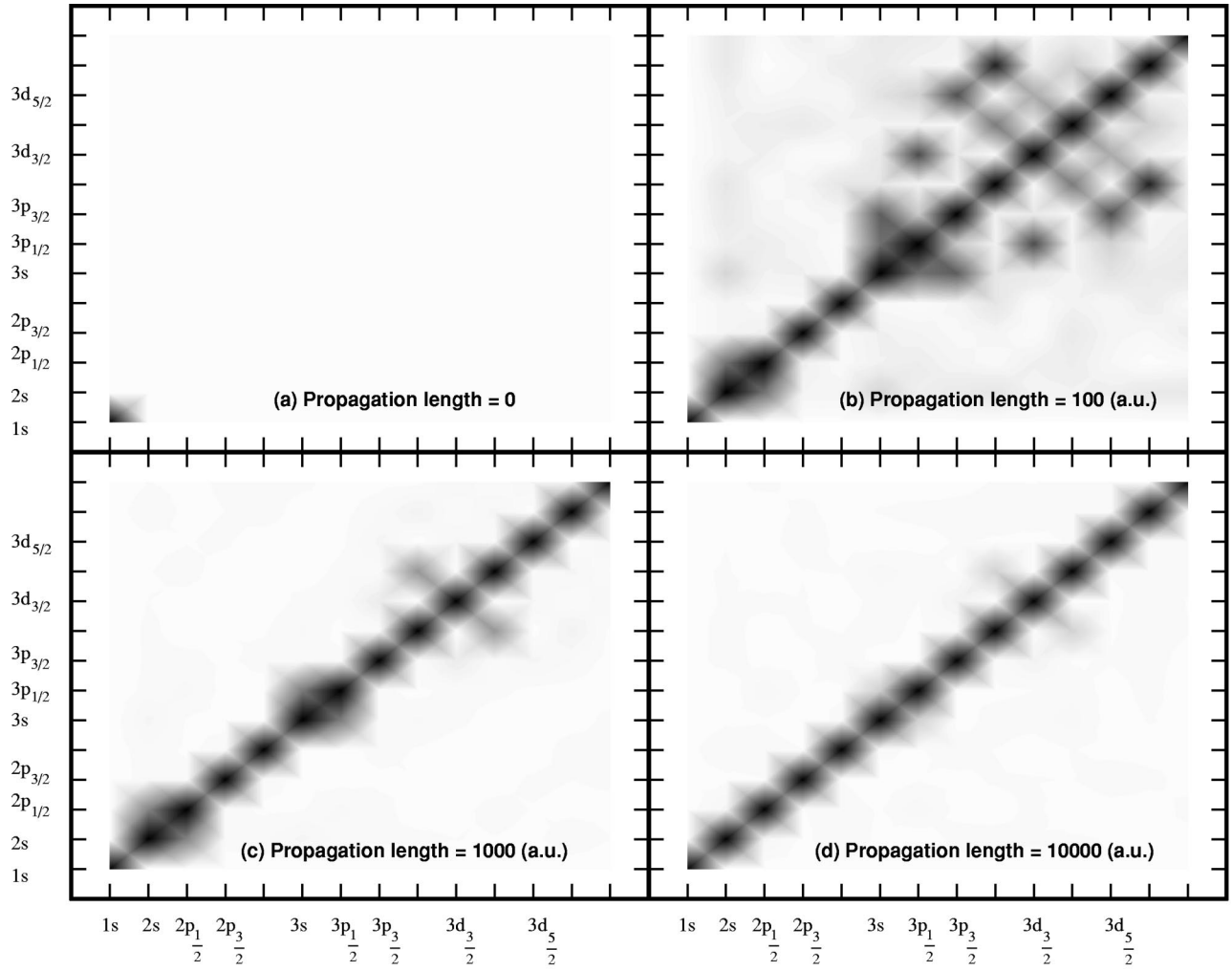

FIG. 7. Density plots of relative coherences of the reduced density matrix of the internal state of a Kr^{35+} ion moving with velocity $v_p=47$ a.u. subject to collisions with screened nuclei in an amorphous carbon foil for various propagation lengths. The system is initially prepared in a statistical incoherent superposition of the $1s_{1/2,-1/2}$ and $1s_{1/2,1/2}$ states (only matrix elements involving $m_j<0$ states are shown).

$$P^{(\ell)\eta}=\frac{\langle\Psi^{\eta}(t)|\Gamma^{(\ell)}|\Psi^{\eta}(t)\rangle}{\sum_{\ell'}\langle\Psi^{\eta}(t)|\Gamma^{(\ell')}|\Psi^{\eta}(t)\rangle}. \tag{5.4}$$

After the channel index ℓ is selected by drawing a random number according to Eq. (5.4), the wave function after the stochastic jump is obtained by application of the corresponding normalized jump operator, Eq. (2.15), for the particular selected channel [i.e., using Eqs. (4.8), (4.19), or (4.37)]. Application of the jump operator requires the determination of a particular value of $\vec{k}$ according to Eq. (2.16). For radiative decay this corresponds to a discrete distribution of the index $\mathfrak{z}$ whereas for collisions it corresponds to continuous two-dimensional and three-dimensional probability densities for $\vec{k}_\perp$ and $\vec{k}$ for electron-core and e-e interactions, respectively.

B. Application to Kr^{35+} traversing amorphous carbon foils

We consider now the QTMC simulation for $Kr^{35+}(1s)$ traversing amorphous carbon foils. Experimental and theoretical studies for this system have been reported elsewhere [4]. The ion is initially prepared in a statistical incoherent superposition of $1s$ states and is traveling at the speed $v_p=47$ a.u. The Kr isotopes used in the experiments are chosen such that the hyperfine structure of the ion can be ignored. The fine-structure Hamiltonian $H_S^{(v)}$ [Eq. (4.12)] is therefore adequate.

In order to probe the time evolution of the internal state of the ion, Balmer α lines are measured for foils of different thicknesses that vary from 3 to 220 $\mu g/cm^2$. The total photon intensity of all lines emitted from a particular level is given by

$$I_\alpha=\Gamma_\alpha^{(r)}\int_0^\infty dt\,\sigma_{\alpha\alpha}(t). \tag{5.5}$$

The intensity provides direct information on the time integral of the population $\sigma_{\alpha\alpha}(t)$ (weighted by a constant decay rate). Note that the time integral involves the population while the ion is both inside the solid and after foil exit.

The population of the excited state is initially zero, increases due to excitation inside the foil, and tends to zero again for $t \to \infty$, when the atom relaxes to the ground state by radiative decay after foil transmission. Since transport through foils of different thickness yield different intermediate populations, changes in the line intensities provide direct evidence of the changing behavior of the populations due to transport. Because energy levels of different m_j are not experimentally resolved, the observable intensities correspond to $I_{n,l,j} = \Sigma_{m_j} I_{n,l,j,m_j}$.

In Eq. (5.5) $|\alpha\rangle$ represents an eigenstate of the free-ion Hamiltonian $H_S^{(v)}$ [Eq. (4.12)]. It is important to note that the system Hamiltonian inside and outside the solid is different. Therefore, the calculation of the dynamics of the internal state of the ion is separated in two parts. First, we propagate the ion inside the foil and the calculation is carried out in a basis set $|\overline{\alpha}\rangle$, $|\overline{\beta}\rangle$, etc., of eigenstates of the system Hamiltonian inside the solid,

$$H_S^{(s)} \equiv -\frac{\nabla_{\vec{r}}^2}{2} - \frac{Z_p}{r} + \Delta H_{rel} + V_{wake}(\vec{r}). \tag{5.6}$$

The Coulomb field of the swift ion polarizes the solid, resulting in a ''wake'' of density fluctuations [34]. This wake acts back on the ion shifting and splitting the internal electronic energy levels. For a highly charged ion the dominant polarization of the solid that affects the time evolution of the internal state of the ion is that due to the nucleus of the ion rather than that of the projectile electron. We therefore include the ion-induced wake potential $V_{wake}(\vec{r})$ in Eq. (5.6). The (conservative) potential $V_{wake}(\vec{r})$ resembles, to leading order and at small distances from the nucleus, an electric field which causes Stark splittings in hydrogenic manifolds. The interaction of the projectile electron with its self-induced polarization described by $\mathrm{Re}(\tilde{G})$ (or χ') is small by comparison and will be neglected in the following. A more detailed explanation of the different ingredients of $H_S^{(s)}$ can be found in Ref. [4]. At the foil exit, the density matrix is projected onto the set of eigenstates $|\alpha\rangle$ of the free-ion Hamiltonian $H_S^{(v)}$ [Eq. (4.12)] and is subsequently propagated in time in that basis.

In Figs. 8(a) and 8(c), the populations of the $3s_{1/2,-1/2}$ and $3p_{1/2,-1/2}$ states as well as the relative coherence $Q_{3s_{1/2,-1/2},3p_{1/2,-1/2}}$ are displayed as a function of the propagation length. (Note that propagation length is equivalent to foil thickness.) The results of the full simulation depicted in Figs. 8(a) and 8(c) are found to be very similar to those involving only core collisions, indicating that much of the dynamics of the system is dominated by core collisions. This is also evident in the density plots of the relative coherences depicted in Fig. 9, which look very similar to those in Fig. 7. Only for large propagation lengths are the results of the full simulation clearly different from those involving only core collisions, which is a consequence of *e-e* collisions and radiative decay. The relative coherence [Fig. 8(c)] is very large for thin foils and is subsequently damped due to multiple collisions.

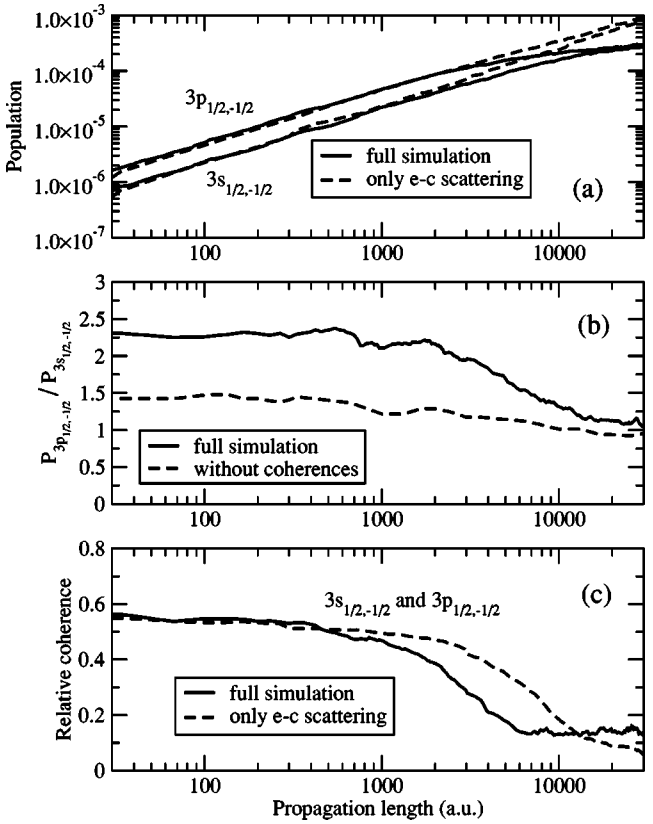

FIG. 8. Evolution of selected populations and coherences of the internal state of a Kr^{35+} ion traversing an amorphous carbon foil with velocity $v_p = 47$ a.u. as a function of the propagation length. The system is initially prepared in a statistical incoherent superposition of the $1s_{1/2,-1/2}$ and $1s_{1/2,1/2}$ states and we compare the results of the full simulation with those in Fig. 6. (a) Populations of the $3s_{1/2,-1/2}$ and $3p_{1/2,-1/2}$ states, (b) ratio of the $3p_{1/2,-1/2}$ population to the $3s_{1/2,-1/2}$ population, and (c) relative coherence between the $3s_{1/2,-1/2}$ and $3p_{1/2,-1/2}$ states.

In order to analyze the effect of collisional coherences on the populations of the states, we also display in Fig. 8(b) results of simulations with and without collisional coherences. The QTMC method easily allows us to eliminate coherences by making the decay matrices diagonal and by multiplying the matrix elements of the jump operator in the basis set that diagonalizes the system Hamiltonian by random phases uniformly distributed in the interval $(0,2\pi)$. In order to highlight the differences between the simulations, Fig. 8(b) displays the ratio between the populations of the $3p_{1/2,-1/2}$ and $3s_{1/2,-1/2}$ states with and without coherences included. For thin foils, the population ratio is nearly constant, reflecting the ratios of direct transition probabilities from the ground state of Kr to different final states under single-collision conditions. Subsequently, it decreases to a value close to unity. Without coherences, the simulation reaches this asymptotic ratio much faster. Similar effects occurs in the absence of the wake field [4]. This is due to the fact that for the relative phases associated with the excitation process, the wake field tends to increase the ratio of the $3p_{1/2}$ population to the $3s_{1/2}$ population.

Direct experimental evidence of coherences can be ob-

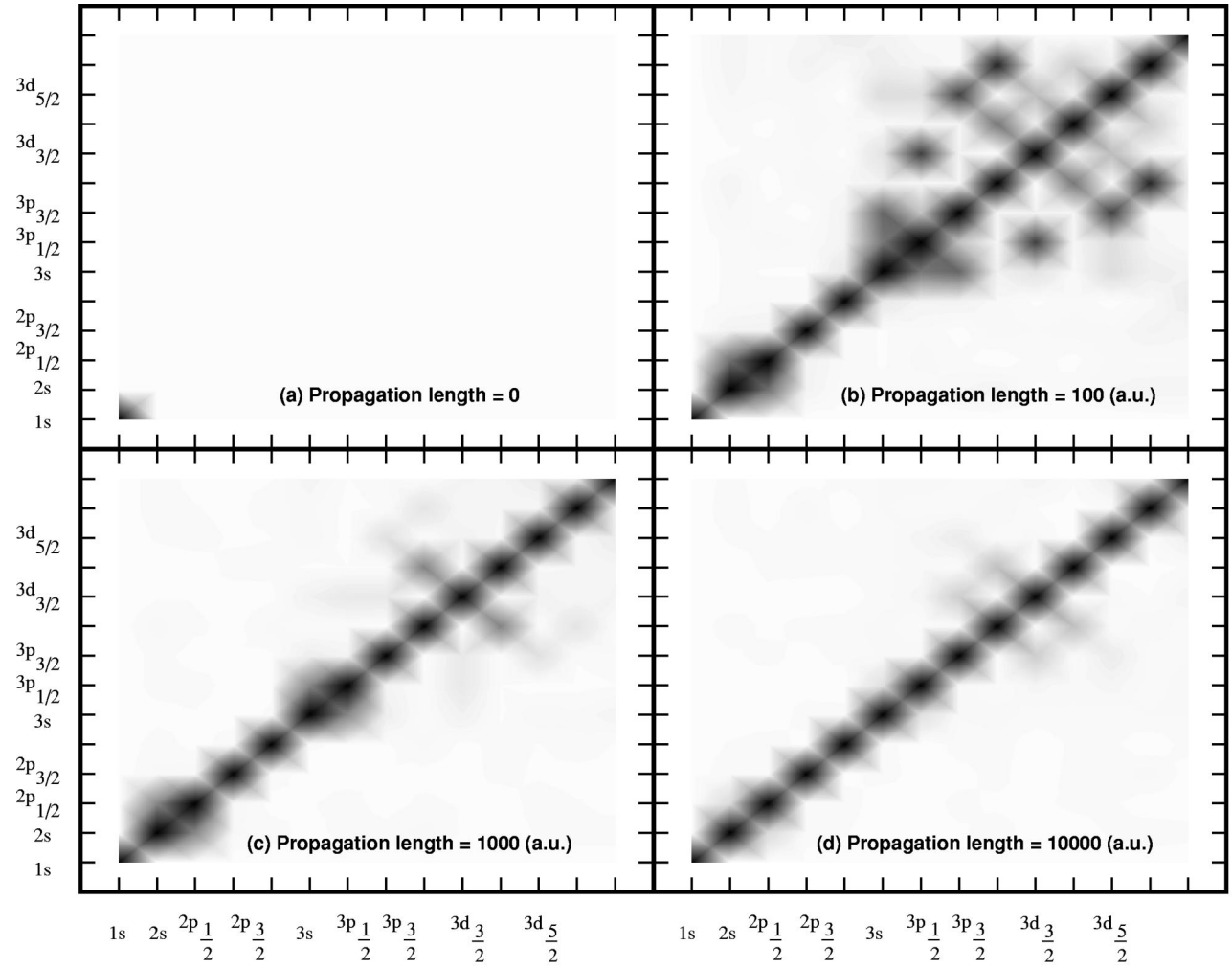

FIG. 9. Density plots at various propagation lengths of relative coherences of the reduced density matrix of the internal state of a Kr^{35+} ion traversing and amorphous carbon foil with velocity $v_p=47$ a.u. and subject to radiative decay, e-e collisions and core collisions. The system is initially prepared in a statistical incoherent superposition of the $1s_{1/2,-1/2}$ and $1s_{1/2,1/2}$ states (only matrix elements involving m_j <0 states are shown).

tained by measuring ratios of line emission intensities [1]. In Fig. 10 we compare the results of our simulations with and without collisional coherences and experimental data for the ratio $I_{3p_{1/2}}/I_{3s_{1/2}}$. Only inclusion of collisional coherences leads to the correct degree intrashell mixing of states and yields photon intensities that are in reasonable agreement with the experimental data. It is also worth noting that the calculated ratio $I_{3p_{1/2}}/I_{3s_{1/2}}$ obtained from the full simulation including post-foil evolution increases for increasing foil thickness, whereas the ratio of the populations at the foil exit [Fig. 8(b)] are a decreasing function of foil thickness. This is a direct consequence of radiative decay during the transport in the foil.

In our previous work [4], numerical simulations yielded slighly better agreement with the experimental data in the thick-foil region than that in Fig. 10. This observation is at first glance somewhat surprising since for the limiting case of highly excited states (which will be discussed in the following section) our previous approach is based on additional approximations to the present theory. Comparison of the present jump operators, continuous time evolution operators, and jump times with those in Ref. [4] indicates that the present approach differs from the previous one in several details entering the QTMC simulations. These differences do not yield dramatically different results for the present system but they could be of importance for other systems (for example, the model used in Ref. [4] for radiative decay did not describe the buildup of coherences due to the interaction with the environment). While the slightly better agreement between our previous calculations and experiment in the thick-foil region may be, in part, fotuitous, there is one possible source of the discrepany that warrants further investigation. The present QTMC implementation is strictly unitary as is the underlying Lindblad equation it solves by way of ensemble averages. In other words, there exists no flow of probability from the finite Hilbert subspace $\mathbb{H}_S$ spanned by the basis set to its complement (i.e., we have neglected the flow of probability from low-n states to high-n and continuum states). In our previous work we provided an intuitive way to account for this flow (while neglecting the back flow)

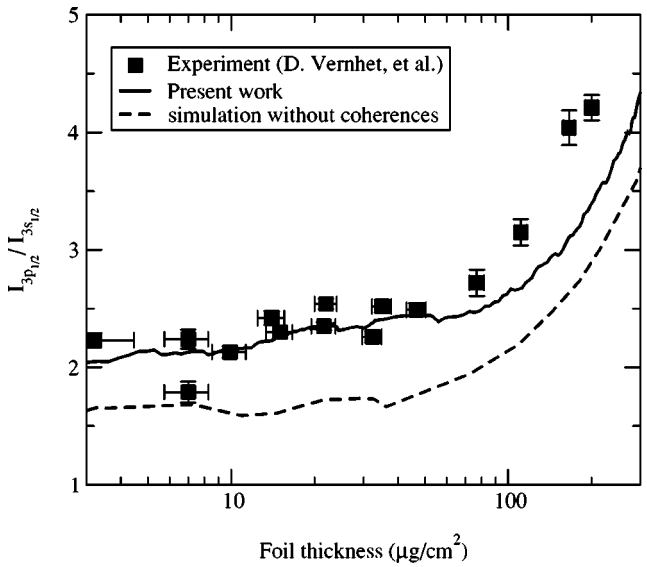

FIG. 10. Relative line emission intensities resulting from the transmission of Kr^{35+} ions through amorphous carbon foils with velocity $v_p=47$ a.u. as a function of the foil thickness. The system is initially prepared in a statistical incoherent superposition of the $1s_{1/2,-1/2}$ and $1s_{1/2,1/2}$ states. The results of our full simulation are compared with experimental data [4] and with a simulation in which coherences are neglected.

and it was found to have a small effect in the thick foil region. The derivation of a generalized ''Lindblad'' form that accounts for this flow and its QTMC solution is in progress.

C. Transport of Rydberg states: Linear stochastic Schrödinger equation

We consider now the limit of the NLSSE when the initial state of the projectile is in a highly excited or Rydberg state ($n \gg 1$). As radiative decay rates decrease as n^{-x} ($x=3$ to 4.5) while collisional rates for charged particles rapidly increase for low n as $\sim n^2$ and saturate for large n, only collisional relaxation is important. In this limit, the NLSSE drastically simplifies and reduces to a linear equation. The key point is that the dependence of the susceptibility χ''_+ on the internal energy differences $\omega_{\alpha\nu}$ can be neglected compared to the magnitude of the Doppler shift, $|kv_p|$ and Eq. (3.34) becomes

$$S_{\alpha\beta}(\vec{k}) \simeq f(\vec{k}) W_{\alpha\beta}(\vec{k}) [2\chi''_+(\vec{k}, -\vec{k}\cdot\vec{v}_p)]^{1/2}. \quad (5.7)$$

Consequently, decay matrix (2.14) simplifies to

$$\Gamma_{\alpha\beta} = \frac{1}{V} \sum_{\vec{k}} |f(\vec{k})|^2 \chi''_+(\vec{k}, -\vec{k}\cdot\vec{v}_p) \langle \alpha | W^\dagger(\vec{k}) W(\vec{k}) | \beta \rangle. \quad (5.8)$$

For e-e and core collisions $W=\exp(i\vec{k}\cdot\vec{r})$ and $W^\dagger(\vec{k})W(\vec{k})=1$. Therefore, we arrive at

$$\Gamma_{\alpha\beta} = \delta_{\alpha\beta} \frac{1}{V} \sum_{\vec{k}} |f(\vec{k})|^2 \chi''_+(\vec{k}, -\vec{k}\cdot\vec{v}_p) = \gamma \delta_{\alpha\beta}, \quad (5.9)$$

which is not only diagonal but proportional to the unit matrix and with the scattering rate γ for free electrons as prefactor. Thus, the approximation $\omega_{\alpha\nu} \to 0$ amounts to the so-called quasi-free-electron approximation for weakly bound electrons. The fact that Γ is state independent has profound consequences for the resulting stochastic time evolution. The continuous unitary evolution operator [Eqs. (2.12) and (2.13)] becomes independent of Γ,

$$U_{cont}(t_j, t_{j-1}) = \exp[-iH_S(t_j - t_{j-1})]. \quad (5.10)$$

Similarly, using Eq. (5.7) in the definition of the jump operator Eq. (2.15) yields

$$U_{jump}(\vec{k_j}, t_j) = \exp(i\vec{k}_j \cdot \vec{r}). \quad (5.11)$$

Note that we have dropped the index η in Eqs. (5.10) and (5.11) since these operators are in this limit independent of the particular realization of the quantum trajectory. Both U_{cont} and U_{jump}, as well as their product Eq. (2.11) reduce to linear operators. Consequently, the time evolution of the quantum trajectory is governed by a *linear* Schrödinger equation $id|\Psi(t)\rangle/dt = H|\Psi(t)\rangle$ generated by the stochastic Hamiltonian

$$H(t) = H_S - \sum_j \delta(t - t_j) \vec{r}\cdot\vec{k}_j, \quad (5.12)$$

where the random jump times t_j and momentum transfers k_j are obtained from Eqs. (2.19) and (2.16), which in the quasi-free-electron approximation reduce to $u=1-\exp(\gamma t)$, and $P(\vec{k}) = \gamma^{-1}|f(\vec{k})|^2 \chi''_+(\vec{k}, -\vec{k}\vec{v}_p)$, respectively.

Equation (5.12) is nothing but the Hamiltonian of an impulsively driven atom, a system frequently studied in the connection of quantum chaos [37–42] and of Rydberg atoms perturbed by half-cycle pulses (Refs. [43,44]). Equation (5.12) possesses a well-defined classical limit in terms of Hamilton equations of motion and allows to treat the problem also within the realm of classical mechanics. In this limit we recover the Langevin-type equations of motion underlying the classical transport theory [9–14] and applicable to transport of weakly bound and continuum electrons. The previously developed quantum transport theory for internal state evolution in ion-solid interactions (Refs. [16,17]) was based on Eq. (5.12). The present analysis shows it to be the limiting case of a NLSSE when the quasi-free approximation [Eq. (5.7)] can be applied. For light ions and high Rydberg states of highly charged ions the quasi-free-electron approximation is valid to a good degree of approximation.

It is worth noting that this linear limit of the NLSSE is specific to collisions. For radiative processes, the susceptibility $\chi''_+ \sim |\omega_{\alpha\beta}|$ [Eq. (4.6)] vanishes in the limit $\omega_{\alpha\beta} \to 0$. Therefore the assumption of a, to leading order, frequency-independent χ''_+ which would allow the use of a closure relation and of the unitarity of W [see Eq. (5.7) and (5.8)] fails. From another angle, radiative transition probabilities are strongly state dependent and an approximation of state independence in analogy to the quasi-free-electron approximation for electron scattering (5.7) is not possible.

VI. CONCLUSIONS

In this work we have derived from first principles a general method based on the Lindblad equation and its quantum-trajectory Monte Carlo implementation to describe the dynamics of fast atoms or ions interacting with a large environment consisting of the electromagnetic field and a solid. One major advantage of the present formulation is that is goes beyond the secular approximation and can account for the short time evolution of the coherences of the system. The present treatment contains our previous approximation (e.g., Ref. [4]) as the limiting case when the nonlinear stochastic Schrödinger equation reduces to a linear stochastic equation. We show that this limit emerges from the quasi-free-electron approximation to electron-electron and electron-core scattering. The results obtained in this work for line emission intensities resulting from ion-solid interactions resemble those found in our previous work and, therefore, partially validate our previous approach. However, significant differences, in particular for the radiative decay, arise.

One major conclusion from our present treatment is that the interaction with the environment does not only decohere a quantum state in the long-time limit but also can lead to a buildup of coherences on an intermediate time scale given by the inverse of a frequency spacing between closely lying levels of the system. While the present method was developed with the goal to treat internal-state evolution during the penetration through solids, it is equally applicable to other atomic systems in contact with an environment. Examples for future studies include Rydberg atoms in a trap envisioned as gates and registers for quantum information processing. In this case, stray fields, collisions with ambient molecules, and the radiation field represent the environment [45].

One major limitation of the present approach should be pointed out. One virtue of the Lindblad equation and its QTMC implementation, the strictly unitary time transformation of the reduced density-matrix $\sigma(t)$ is, in fact, of limited value when the atomic system couples to the continuum that cannot be completely subtended within any realistic basis size. In other words, when the atomic Hilbert subspace $\mathbb{H}_S$ represented by the N_S dimensional basis is strongly coupled to its complement, unitarity is not preserved nor should it be since there is net flux out of the reduced Hilbert space. The present formulation of the Lindblad equation and its QMTC implementation does not account for an explicitly nonunitary evolution of the system. As the ionization channel becomes increasingly important for lower Z_p, extension of the present formulation to explicitly nonunitary system dynamics is planned.

ACKNOWLEDGMENTS

This work was supported by the NSF and FWF (Austria). C.O.R. acknowledges support by the DCS, OBES, USDOE, managed by UT-Battelle, LLC, under Contract No. DE-AC05-00OR22725.

[1] D. Vernhet, J-P. Rozet, I. Bailly-Despiney, C. Stephan, A. Cassimit, J-P. Grandin, and L.J. Dubé, J. Phys. B **31**, 117 (1998).
[2] D. Vernhet, J.P. Rozet, E. Lamour, B. Gervais, C. Fourment, and L.J. Dubé, Phys. Scr., T **T80A**, 83 (1999).
[3] P. Nicolai, M. Chabot, J.P. Rozet, M.F. Politis, A. Chetioui, C. Stéphan, A. Touati, D. Vernhet, and K. Wohrer, J. Phys. B **23**, 3609 (1990).
[4] T. Minami, C.O. Reinhold, M. Seliger, J. Burgdörfer, C. Fourment, B. Gervais, E. Lamour, J-P. Rozet, and D. Vernhet, Phys. Rev. A **65**, 032901 (2002).
[5] N. Bohr and L. Lindhard, K. Dan. Vidensk. Selsk. Mat. Fys. Medd. **26**, 12 (1954).
[6] R. Zwanzig, J. Chem. **33**, 1338 (1960).
[7] J. Prigogine and P. Resibois, Physica (Utrecht) **27**, 629 (1961).
[8] H. Gabriel, Phys. Rev. **181**, 506 (1969).
[9] J. Burgdörfer, in *Proceedings of the Third Workshop on High Energy Ion-Atom Collisions*, edited by D. Berenyi and G. Hock, Lecture Notes in Physics Vol. 294 (Springer-Verlag, Berlin, 1988), p. 344.
[10] J. Burgdörfer and J. Gibbons, Phys. Rev. A **42**, 1206 (1990).
[11] J. Burgdörfer and C. Bottcher, Phys. Rev. Lett. **61**, 2917 (1988).
[12] J. Kemmler, J. Burgdörfer, and C.O. Reinhold, Phys. Rev. A **44**, 2993 (1991).
[13] C.O. Reinhold, J. Burgdörfer, J. Kemmler, and P. Koschar, Phys. Rev. A **45**, R2655 (1992).
[14] B. Gervais, C.O. Reinhold, and J. Burgdörfer, Phys. Rev. A **53**, 3189 (1996).
[15] P. Kürpick, C.O. Reinhold, J. Burgdörfer, and B. Gervais, Phys. Rev. A **58**, 2183 (1998).
[16] C.O. Reinhold, M. Melles, H. Shao, and J. Burgdörfer, J. Phys. B **26**, L659 (1993); **29**, 377 (1996).
[17] D.G. Arbó, C.O. Reinhold, S. Yoshida, and J. Burgdörfer, Nucl. Instrum. Methods Phys. Res. B **164-165**, 495 (2000).
[18] J. Dalibard, Y. Castin, and K. Mølmer, Phys. Rev. Lett. **68**, 580 (1992); K. Mølmer, Y. Castin, and J. Dalibard, J. Opt. Soc. Am. B **10**, 524 (1993).
[19] R. Dum, P. Zoller, and H. Ritsch, Phys. Rev. A **45**, 4879 (1992).
[20] H.J. Carmichael, Phys. Rev. Lett. **70**, 2273 (1993).
[21] C.W. Gardiner and P. Zoller, *Quantum Noise* (Springer, New York, 1999).
[22] G. Lindblad, Commun. Math. Phys. **48**, 119 (1976); G. Lindblad, Rev. Mod. Phys. **10**, 393 (1976).
[23] U. Weiss, *Quantum Dissipative Systems* (World Scientific, Singapore, 1999).
[24] L. Diosi, Europhys. Lett. **22**, 1 (1993).
[25] A. Suarez, R. Silbey, and I. Oppenheim, J. Chem. Phys. **97**, 5101 (1992).
[26] W. Pollard and R. Friesner, J. Chem. Phys. **100**, 5054 (1994).
[27] P. Pechukas, Phys. Rev. Lett. **73**, 1060 (1994).
[28] D. Kohen, C. Marston, and D. Tannor, J. Chem. Phys. **107**, 5236 (1997).
[29] A.G. Redfield, IBM J. Res. Dev. **1**, 19 (1957); Adv. Magn. Reson. **1**, 1 (1965).
[30] C. Cohen-Tannoudji, J. Dupont-Roc, and G. Grynberg, *Atom-*

Photon Interactions (Wiley Interscience, New York, 1992).
[31] K. Blum, *Density Matrix Theory and Applications* (Plenum, NY, 1981).
[32] W. Louisell, *Quantum Coherence Properties of Radiation* (Wiley, NY, 1973).
[33] R. Blümel, A. Buchleitner, R. Graham, L. Sirko, U. Smilansky, and H. Walther, Phys. Rev. A **44**, 4521 (1991).
[34] P.M. Echenique, W. Brandt, and R.H. Ritchie, Phys. Rev. B **33**, 43 (1979).
[35] D. Pines and P. Nozieres, *Theory of Quantum Liquids* (Addison–Wesley, Reading, 1989).
[36] C. Martin, E. Arakawa, T. Callcott, and J. Ashley, J. Electron Spectrosc. Relat. Phenom. **35**, 307 (1985); J. Ashley, J. Cowan, R. Ritchie, V.E. Anderson, and J. Hoelzel, Thin Solid Films **60**, 361 (1979); J. Ashley, J. Electron Spectrosc. Relat. Phenom. **28**, 177 (1982).
[37] A. Dhar *et al.*, J. Phys. B **16**, L17 (1983).
[38] A. Carnegie, J. Phys. B **17**, 3435 (1984).
[39] T. Grozdanov and H.S. Taylor, J. Phys. A **20**, 3683 (1987).
[40] J. Burgdörfer, Nucl. Instrum. Methods Phys. Res. B **42**, 500 (1989); M. Melles *et al.*, *ibid.* **79**, 109 (1993).
[41] C.F. Hillermeier *et al.*, Phys. Rev. A **45**, 3486 (1992).
[42] G. Casati *et al.*, Phys. Rev. A **50**, 5018 (1994); H. Wiedermann *et al.*, *ibid.* **49**, 1171 (1994).
[43] M.T. Frey *et al.*, Phys. Rev. A **53**, R2929 (1996).
[44] C.O. Reinhold *et al.*, Phys. Rev. Lett. **79**, 5226 (1997); M.T. Frey *et al.*, Phys. Rev. A **59**, 1434 (1999).
[45] S. Yoshida, S. Watanabe, C.O. Reinhold, and J. Burgdörfer, Phys. Rev. A **60**, 1113 (1999).